













Curved and expanding spacetime geometries in Bose-Einstein condensates

Mireia Tolosa-Simeón ^{1,2,*} Álvaro Parra-López ^{1,3,†} Natalia Sánchez-Kuntz ^{1,‡} Tobias Haas ^{1,4,§} Celia Viermann ^{5,||}
 Marius Sparn ^{5,||} Nikolas Liebster ^{5,||} Maurus Hans ^{5,||} Elinor Kath ^{5,||} Helmut Strobel ^{5,||} Markus K. Oberthaler ^{5,||}
 and Stefan Floerchinger ^{1,6,¶}

¹*Institut für Theoretische Physik, Universität Heidelberg, Philosophenweg 16, 69120 Heidelberg, Germany*

²*Institut für Theoretische Physik III, Ruhr-Universität Bochum, 44801 Bochum, Germany*

³*Departamento de Física Teórica and IPARCOS, Facultad de Ciencias Físicas, Universidad Complutense de Madrid, Ciudad Universitaria, 28040 Madrid, Spain*

⁴*Centre for Quantum Information and Communication, École polytechnique de Bruxelles, CP 165/59, Université libre de Bruxelles, 1050 Brussels, Belgium*

⁵*Kirchhoff-Institut für Physik, Universität Heidelberg, Im Neuenheimer Feld 227, 69120 Heidelberg, Germany*

⁶*Theoretisch-Physikalisches Institut, Friedrich-Schiller-Universität Jena, Max-Wien-Platz 1, 07743 Jena, Germany*



(Received 22 February 2022; accepted 24 August 2022; published 14 September 2022)

Phonons have the characteristic linear dispersion relation of massless relativistic particles. They arise as low-energy excitations of Bose-Einstein condensates and, in nonhomogeneous situations, are governed by a space- and time-dependent acoustic metric. We discuss how this metric can be experimentally designed to realize curved spacetime geometries, in particular, expanding Friedmann-Lemaître-Robertson-Walker cosmologies, with negative, vanishing, or positive spatial curvature. A nonvanishing Hubble rate can be obtained through a time-dependent scattering length of the background condensate. For relativistic quantum fields, this leads to the phenomenon of particle production, which we describe in detail. We explain how particle production and other interesting features of quantum field theory in curved spacetime can be tested in terms of experimentally accessible correlation functions.

DOI: [10.1103/PhysRevA.106.033313](https://doi.org/10.1103/PhysRevA.106.033313)

I. INTRODUCTION

When studying quantum field theory in curved spacetime, many interesting phenomena and peculiarities arise. Most prominently, allowing for a time-dependence in the metric, which is naturally the case in cosmology, leads to the phenomenon of particle production [1–4]. Although indirect signatures of this effect can be observed, for example, in the cosmic microwave background, any direct detection is an open challenge.

In recent years, an analogy of this phenomenon has been studied in the context of Bose-Einstein condensates (BECs) as an integral part of the analog gravity program (see Refs. [5–7] for introductions). More precisely, the linear phononic excitations on top of the ground state of a BEC obey a Klein-Gordon equation for a scalar quantum field in curved spacetime in the acoustic approximation (that is neglecting quantum pressure) [8]. The corresponding metric is the so-called *acoustic metric* (see also Refs. [9,10] for early developments in the context of fluids) and is fully determined by the back-

ground parameters of the BEC, such as the background density or the speed of sound. In this manner, the condensate shapes the spacetime geometry experienced by the acoustic excitations.

It has been shown that introducing suitable time dependencies of either the scattering length or the external trapping potential allow for a one-to-one mapping of the acoustic metric onto spatially flat Friedmann-Lemaître-Robertson-Walker (FLRW) metrics [11–21]. In this sense, all phononic modes propagate in a spacetime geometry set by the acoustic metric with the same speed of sound. In this way, modern cold atom experiments allow for a direct analysis of quantum effects in the context of cosmological models.

Further theoretical studies in this direction have included quantum pressure leading to a quadratic dispersion relation in the ultraviolet momentum regime and so-called rainbow FLRW metrics [19,22]. Two-component BECs allowing for an additional massive phononic mode have also been investigated [23,24]. Recent experimental efforts for simulating an expanding universe in $d = 1 + 1$ effective spacetime dimensions [25] in the laboratory can be found in Refs. [26,27].

Other interesting phenomena that have been studied within the acoustic metric approach (also experimentally) comprise sonic black holes [9,10,28–31], the Unruh effect [32–34], Hawking radiation [35–38], or the dynamical Casimir effect [39]. For an overview over current experimental approaches, see Ref. [40].

*tolosa@tp3.rub.de

†alvaparr@ucm.es

‡sanchez@thphys.uni-heidelberg.de

§tobias.haas@ulb.be

||curvedspacetime@matterwave.de

¶stefan.floerchinger@uni-jena.de

In this paper, we focus on the analogy between the acoustic metric and the FLRW metric for an effectively $d = 2 + 1$ dimensional isotropic trap, which is a common setup of modern BEC experiments. In contrast to previous works, we derive the acoustic metric by parametrizing the quantum fluctuations on top of the ground state in terms of the real and imaginary parts of the complex nonrelativistic scalar field, instead of magnitude and complex phase (see, e.g., Refs. [41,42] for a detailed discussion regarding this parametrization).

We generalize previous studies from spatially flat to spatially curved spacetimes. To this end, we explicitly consider radial dependencies of the background density profile. We find mappings between FLRW universes of positive and negative spatial curvature and the acoustic metric.

After allowing, additionally, for a time-dependent scattering length, we analyze particle production in different types of expanding cosmologies. In this sense, we extend on earlier considerations by providing an exact mapping to a more general class of cosmologies and by showing how the effect of particle production is accessible experimentally. Note that some technical details on the cosmology side are provided in our companion paper [43].

The remainder of this paper is organized as follows. In Sec. II, we introduce isotropic traps in a quasi-two-dimensional geometry and make an ansatz for the quantum effective action. We derive conditions on the background parameters such that the background density remains static. We also compute the acoustic metric from the effective action for the fluctuations and discuss the external potentials required for a one-to-one mapping between the acoustic metric and FLRW metrics of positive and negative curvature. Thereupon, we investigate the properties of the arising FLRW universes by comparing the dynamics of radially outmoving phonons. In Sec. III, we derive a formalism for the spectrum of fluctuations and the two-point correlation function of a rescaled density contrast for different types of (spatially curved) cosmologies. We study both quantities in Sec. IV for various experimentally accessible scenarios and point out robust features. Finally, we give a résumé and formulate an outlook in Sec. V.

Notation. In this paper, we work in SI units. For convenience, we use operator hats for creation and annihilation operators and drop them otherwise. Greek indices μ, ν run from 0 to 2, while latin indices i, j only run from 1 to 2. Also, vectors are denoted by bold symbols.

II. ACOUSTIC METRIC IN 2D ISOTROPIC TRAPS

In the first part of this paper, we discuss the acoustic metric and how it can be mapped to curved FLRW metrics for a quasi-two-dimensional BEC that is confined in an isotropic trap.

A. Quasi-two-dimensional geometry and quantum effective action

Let us begin our analysis with the quantum effective action of a nonrelativistic complex scalar field equipped with a quartic contact interaction term. This is an accurate description for the dynamics of a BEC, i.e., a weakly coupled Bose gas,

where most atoms occupy the ground state. We denote the bosonic field expectation value (in general in the presence of sources) in $d = 3 + 1$ spacetime dimensions by $\psi(t, \mathbf{r})$. We consider a pancake-type geometry in cylindrical coordinates (r, φ, z) and a condensate that is tightly confined in the z direction. Then the extension of the condensate in z direction l_z is much smaller than in the longitudinal direction l_r , i.e., $l_z \ll l_r$, leading to a quasi- $d = 2 + 1$ dimensional geometry. Due to the strong confinement in the z direction, the motional degrees of freedom in this direction are frozen in, such that the mean field $\psi(t, \mathbf{r})$ separates according to $\psi(t, \mathbf{r}) = \Phi(t, r, \varphi)\zeta(z)$, where $\zeta(z)$ is typically of Gaussian form.

We study the dynamics of the field $\Phi(t, \mathbf{r})$ in effectively $d = 2 + 1$ spacetime dimensions. Then, the ansatz for the action reads [41]

$$\Gamma[\Phi] = \int dt d^2r \left\{ i\hbar\Phi^*(\partial_t + iA_0)\Phi - \frac{\hbar^2}{2m}(\nabla - i\mathbf{A})\Phi^*(\nabla + i\mathbf{A})\Phi - \frac{\lambda}{2}(\Phi^*\Phi)^2 \right\}. \quad (1)$$

Here, m denotes the mass of the atoms and $\lambda = \lambda(t)$ is a time-dependent coupling, which can be expressed in terms of the s -wave scattering length $a_s(t)$ within Born's approximation [44],

$$\lambda(t) = \sqrt{\frac{8\pi\omega_z\hbar^3}{m}}a_s(t), \quad (2)$$

where ω_z is the trapping frequency in the z direction.

Furthermore, we introduced an external U(1) gauge field $A = (A_0, \mathbf{A})$ such that there is a symmetry of the action $\Gamma[\Phi]$ under the local U(1) transformation

$$\begin{aligned} \Phi(t, \mathbf{r}) &\rightarrow e^{-i\alpha(t, \mathbf{r})}\Phi(t, \mathbf{r}), \\ A_0(t, \mathbf{r}) &\rightarrow A_0(t, \mathbf{r}) + \partial_t\alpha(t, \mathbf{r}), \\ \mathbf{A}(t, \mathbf{r}) &\rightarrow \mathbf{A}(t, \mathbf{r}) + \nabla\alpha(t, \mathbf{r}). \end{aligned} \quad (3)$$

An external trapping potential is then given by $A_0(t, \mathbf{r}) = V(t, \mathbf{r})/\hbar$. In our analysis, we restrict to isotropic trapping potentials of the form

$$V(t, r) = \frac{m}{2}\omega^2(t)f(r), \quad (4)$$

where $\omega(t)$ is a time-dependent parameter and $f(r)$ is typically a polynomial in r . Without loss of generality, we can assume $f(0) = 0$. For example, $f(r) = r^2$ corresponds to the commonly used harmonic trap, in which case $\omega(t)$ plays the role of a trapping frequency. Moreover, in chemical equilibrium the chemical potential would enter A_0 such that $A_0(t, \mathbf{r}) = (V(t, \mathbf{r}) - \mu)/\hbar$.

In the following, we will work with a linear splitting of the fundamental field Φ into a background part ϕ_0 and a fluctuating part parametrized by two real fields ϕ_1 and ϕ_2 , such that

$$\Phi(t, \mathbf{r}) = \phi_0(t, \mathbf{r}) + \frac{1}{\sqrt{2}}[\phi_1(t, \mathbf{r}) + i\phi_2(t, \mathbf{r})]. \quad (5)$$

Therein, we allowed for general space and time dependencies for all fields. In the present paper, we do not consider any explicit backreaction of fluctuations to the form of the action.

The fluctuations are assumed to be small enough and will be kept only to linear order in equations of motion corresponding to quadratic order in the action. Conceptually, this corresponds to a background field which is well described by mean field equations. We will also not consider any renormalization of the couplings in the action. In this sense, the action Eq. (1) can actually be identified with (an approximation of) the quantum *effective* action, which is renormalized already.

We are particularly interested in evaluating the effective action at the point where the field equation of motion is satisfied:

$$\frac{\delta}{\delta\Phi(t, \mathbf{r})} \Gamma[\Phi] = 0. \quad (6)$$

The background field $\phi_0(t, \mathbf{r})$ corresponds then to an expectation value of the microscopic field or quantum operator in the absence of sources (up to a wave function renormalization constant). The normalization implicit in Eq. (1) is such that $n_s = |\Phi|^2$ is the superfluid density, which at vanishing temperature equals the full density $n = n_s$. For $A_0 = V/\hbar$ and $\mathbf{A} = 0$, the classical field $\phi_0(t, \mathbf{r})$ is a solution of the Gross-Pitaevskii equation [45,46]

$$i\hbar\partial_t\phi_0 = \left(-\frac{\hbar^2}{2m}\nabla^2 + V + \lambda|\phi_0|^2 \right)\phi_0. \quad (7)$$

The superfluid behavior of the condensate mean field $\phi_0(t, \mathbf{r})$ can be highlighted by introducing the Madelung representation [47],

$$\phi_0(t, \mathbf{r}) = \sqrt{n_0(t, \mathbf{r})}e^{iS_0(t, \mathbf{r})}, \quad (8)$$

with $n_0(t, \mathbf{r}) = |\phi_0(t, \mathbf{r})|^2$ denoting the background particle number density and $S_0(t, \mathbf{r})$ being the background phase of the condensate's mean field. Using the parametrization (8) in Eq. (7) leads to a pair of hydrodynamic equations, namely, one obtains the local conservation law or continuity equation

$$0 = \partial_t n_0 + \nabla \cdot (n_0 \mathbf{v}), \quad (9)$$

and the Euler equation [48]

$$0 = \hbar\partial_t S_0 + V + \lambda n_0 + \frac{\hbar^2}{2m}(\nabla S_0)^2. \quad (10)$$

We introduced the superfluid velocity via

$$\mathbf{v} = \frac{\hbar}{m}\nabla S_0, \quad (11)$$

and neglected the quantum pressure term,

$$q = -\frac{\hbar^2}{2m} \frac{\nabla^2 \sqrt{n_0}}{\sqrt{n_0}}, \quad (12)$$

in (10), which is the standard assumption leading to the acoustic approximation [5,8]. Note that q in Eq. (12) is of second order in \hbar , as well as in spatial derivatives, such that it is expected to be subleading for sufficiently smooth density.

The dynamics of the background variables required to mimic FLRW universes for the fluctuating variables will be discussed in Secs. II B and II C, respectively.

B. Stationary background density profile

Although we have allowed for general time dependencies of the trapping potential $V(t, r)$ and the coupling $\lambda(t)$, we are interested in describing situations where the background

density n_0 remains static. Therefore, we do not follow the common scaling ansatz put forward in Ref. [49] but instead require the background velocity to vanish $\mathbf{v} = 0$. As a consequence, we do not need to distinguish between laboratory and comoving coordinates as they agree in static situations. The condition $\mathbf{v} = 0$ renders the continuity equation (9) trivial, while the Euler equation (10) evaluates to

$$0 = -\mu_0(t) + \frac{m}{2}\omega^2(t)f(r) + \lambda(t)n_0(r), \quad (13)$$

where we have introduced the background chemical potential

$$\mu_0(t) = -\hbar\partial_t S_0(t). \quad (14)$$

Equation (13) yields the background density profile

$$n_0(r) = \bar{n}_0 \left(1 - \frac{f(r)}{R^2} \right) = \frac{\mu_0(t)}{\lambda(t)} - \frac{m\omega^2(t)}{2\lambda(t)} f(r). \quad (15)$$

Oftentimes, $f(r)$ is a monotonously increasing function of radius r and the condensate extends up to a radius R such that $r \in [0, R]$, at which the density either drops to zero or takes a constant value. Furthermore, we introduced the constant background density at the center of the trap $\bar{n}_0 = n_0(r=0)$, which is also the proportionality constant between the time-dependent chemical potential $\mu_0(t)$ and the coupling $\lambda(t)$, in mean-field approximation,

$$\mu_0(t) = \bar{n}_0 \lambda(t). \quad (16)$$

The constant \bar{n}_0 is also related to the total particle number N via

$$N = 2\pi \bar{n}_0 \int_0^R dr r \left(1 - \frac{f(r)}{R^2} \right). \quad (17)$$

Moreover, the size parameter R appears in the proportionality constant between the time-dependent parameter $\omega(t)$ and the coupling $\lambda(t)$:

$$\omega^2(t) = \frac{2\bar{n}_0}{mR^2} \lambda(t). \quad (18)$$

If the coupling $\lambda(t)$ is changed over time, the latter condition has to be fulfilled to guarantee a stationary density profile of the form (15).

Let us discuss a couple of choices for the radial dependence of the trap encoded in $f(r)$. For $f(r) = r^2$, we obtain the well-known Thomas-Fermi density profile in a harmonic trap and R corresponds to the Thomas-Fermi radius, while $f(r) = F\theta(r-R)$ with $F \rightarrow \infty$ leads to a homogeneous density profile in the region $r < R$. The latter allows for a mapping to a flat FLRW cosmology, which is discussed in detail in Ref. [18].

As we will show later, spatially curved but homogeneous and isotropic FLRW universes follow from radial dependencies of the trap and density profiles of the form

$$f(r) = \pm 2r^2 - \frac{r^4}{R^2} \quad \text{and} \quad n_0(r) = \bar{n}_0 \left[1 \mp \frac{r^2}{R^2} \right]^2. \quad (19)$$

The time dependence of all involved quantities in the density profile of Eq. (19) (with the upper sign) is sketched in Fig. 1. When reducing the coupling $\lambda(t)$ over time, for example, to half of its initial value, the parameter $\omega(t)$ has to be adjusted according to (18) [the background chemical potential $\mu_0(t)$ follows (16)], such that the density profile remains static. Note

that decreasing the coupling $\lambda(t)$ and adjusting the parameter $\omega(t)$ accordingly over time never breaks the confinement condition $\omega(t) \ll \omega_z$, provided that it is fulfilled initially.

C. Deriving the acoustic metric

As a next step, we consider the dynamics of the fluctuations parametrized by the two real fields ϕ_1 and ϕ_2 introduced

$$\Gamma_2[\phi_1, \phi_2] = \int dt d^2r \left\{ \hbar \phi_2 \partial_t \phi_1 - \frac{\hbar^2}{4m} [(\nabla \phi_1)^2 + (\nabla \phi_2)^2] - \frac{1}{2} \left(\hbar A_0 + \hbar^2 \frac{A^2}{2m} \right) (\phi_1^2 + \phi_2^2) \right. \\ \left. - \frac{\hbar^2}{2m} \mathbf{A} (\phi_1 \nabla \phi_2 - \phi_2 \nabla \phi_1) - \frac{\lambda}{2} (\phi_1, \phi_2) \begin{pmatrix} n_0 + \frac{1}{2} (\phi_0^* + \phi_0)^2 & \frac{1}{2} (\phi_0^* + \phi_0) (i\phi_0^* - i\phi_0) \\ \frac{1}{2} (\phi_0^* + \phi_0) (i\phi_0^* - i\phi_0) & n_0 + \frac{1}{2} (i\phi_0^* - i\phi_0)^2 \end{pmatrix} \begin{pmatrix} \phi_1 \\ \phi_2 \end{pmatrix} \right\}. \quad (21)$$

Terms linear in the fluctuating fields ϕ_1 and ϕ_2 cancel out at the point where the effective action is stationary [cf. Eq. (6)], therefore we only have to consider the quadratic part $\Gamma_2[\phi_1, \phi_2]$.

To relate the linearization for the background field (5) to its Madelung representation (8), we perform a local U(1) gauge transformation of the form

$$\phi_0 + \frac{1}{\sqrt{2}} [\phi_1 + i\phi_2] \rightarrow e^{-iS_0} \left(\phi_0 + \frac{1}{\sqrt{2}} [\phi_1 + i\phi_2] \right), \\ A_0 \rightarrow A_0 + \partial_t S_0, \\ \mathbf{A} \rightarrow \mathbf{A} + \nabla S_0. \quad (22)$$

This transformation redefines the fluctuating fields and rotates the—in general complex—background field ϕ_0 such that it becomes real. If we again take the values before the transformation to be $A_0 = V/\hbar$ and $\mathbf{A} = 0$, then afterward we get

$$A_0 = \frac{V}{\hbar} + \partial_t S_0 \quad \text{and} \quad \mathbf{A} = \nabla S_0, \quad (23)$$

so the effective action for the fluctuations becomes

$$\Gamma_2[\phi_1, \phi_2] = \int dt d^2r \left\{ \hbar \phi_2 \partial_t \phi_1 - \frac{\hbar^2}{4m} [(\nabla \phi_1)^2 + (\nabla \phi_2)^2] \right. \\ \left. - \frac{1}{2} \left(V + \hbar \partial_t S_0 + \hbar^2 \frac{(\nabla S_0)^2}{2m} \right) (\phi_1^2 + \phi_2^2) \right. \\ \left. - \frac{\hbar^2}{2m} (\nabla S_0) (\phi_1 \nabla \phi_2 - \phi_2 \nabla \phi_1) \right. \\ \left. - \frac{\lambda n_0}{2} (3\phi_1^2 + \phi_2^2) \right\}. \quad (24)$$

The latter can be simplified using the Euler equation (10), to wit

$$\Gamma_2[\phi_1, \phi_2] \\ = \int dt d^2r \left\{ -\frac{\hbar^2}{4m} (\nabla \phi_2)^2 - \frac{1}{2} \phi_1 \left(2\lambda n_0 - \hbar^2 \frac{\nabla^2}{2m} \right) \phi_1 \right. \\ \left. + \phi_1 \left[-\hbar \partial_t \phi_2 - \frac{\hbar^2}{m} (\nabla S_0) \nabla \phi_2 - \frac{\hbar^2}{2m} (\nabla^2 S_0) \phi_2 \right] \right\}. \quad (25)$$

In the soft regime, i.e., for small momenta, one can replace $2\lambda n_0 - \hbar^2 \nabla^2 / 2m \rightarrow 2\lambda n_0$, which realizes the acoustic

in Eq. (5). To that end, we expand the effective action (1) around the background solution ϕ_0 to quadratic order in the fluctuating fields ϕ_1 and ϕ_2 , which yields

$$\Gamma[\Phi] = \Gamma[\phi_0] + \text{terms linear in } \phi_1, \phi_2 + \Gamma_2[\phi_1, \phi_2], \quad (20)$$

with

approximation for the fluctuation field [50]. This allows one to integrate out ϕ_1 by evaluating it on its equation of motion, leading to a quadratic effective action for ϕ_2 only. Moreover, we also neglect the term $\nabla^2 S_0$, that is, we assume that the background velocity is constant $\mathbf{v} = \text{const}$, which is indeed fulfilled for the scenarios described in Sec. II B, and we rescale the fluctuating field $\phi \equiv \phi_2 / \sqrt{2m}$, such that it has standard mass dimension of a relativistic scalar field. Then we find

$$\Gamma_2[\phi] = \frac{\hbar^2}{2} \int dt d^2r \left\{ \frac{1}{c^2} (\partial_t \phi)^2 - (\nabla \phi)^2 \right. \\ \left. + \frac{2}{c^2} (\partial_t \phi) \mathbf{v} \cdot \nabla \phi + \frac{1}{c^2} (\mathbf{v} \cdot \nabla \phi)^2 \right\}, \quad (26)$$

where we introduced the time- and space-dependent speed of sound

$$c^2(t, \mathbf{r}) = \frac{\lambda(t) n_0(t, \mathbf{r})}{m}. \quad (27)$$

Finally, the latter effective action can be rewritten as an effective action for a free massless scalar field in a curved spacetime determined by the acoustic metric $g_{\mu\nu}(x)$,

$$\Gamma_2[\phi] = -\frac{\hbar^2}{2} \int dt d^2r \sqrt{g} g^{\mu\nu} \partial_\mu \phi \partial_\nu \phi, \quad (28)$$

where $\sqrt{g} \equiv \sqrt{-\det(g_{\mu\nu})}$. Comparing (26) and (28) reveals that the inverse of the acoustic metric is given by

$$(g^{\mu\nu}) = \begin{pmatrix} -1 & v^j \\ v^i & c^2 \delta^{ij} - v^i v^j \end{pmatrix}, \quad (29)$$

while the metric itself reads

$$(g_{\mu\nu}) = \frac{1}{c^2} \begin{pmatrix} -(c^2 - v^2) & -v_j \\ -v_i & \delta_{ij} \end{pmatrix}. \quad (30)$$

Furthermore, this yields $\sqrt{g} = 1/c^2$.

Also, in the acoustic approximation and for a stationary background ($\mathbf{v} = 0$), we find a simple relation between the fluctuating fields

$$\phi_1 = -\frac{\hbar}{2\lambda(t)n_0(r)} \partial_t \phi_2, \quad (31)$$

showing that ϕ_1 is proportional to the time derivative of ϕ_2 .

D. From an acoustic metric to curved FLRW universes

Restricting ourselves to the scenarios described in Sec. II B, i.e., stationary density profiles for the background density $n_0(r)$ corresponding to $v = 0$, leads to an acoustic line element of the form

$$ds^2 = g_{\mu\nu} dx^\mu dx^\nu = -dt^2 + a^2(t) \left(1 - \frac{f(r)}{R^2}\right)^{-1} (dr^2 + r^2 d\varphi^2), \quad (32)$$

where we defined a time-dependent scale factor

$$a^2(t) \equiv \frac{m}{\bar{n}_0 \lambda(t)}. \quad (33)$$

To reshape the former into a curved FLRW line element, we continue with the particular choice $f(r) = \pm 2r^2 - r^4/R^2$ put forward in Eqs. (19), which yields the line element

$$ds^2 = -dt^2 + a^2(t) \left(1 \mp \frac{r^2}{R^2}\right)^{-2} (dr^2 + r^2 d\varphi^2). \quad (34)$$

We then perform a coordinate transformation for the radial coordinate

$$u(r) = \frac{r}{1 \mp \frac{r^2}{R^2}}, \quad (35)$$

with $u \in [0, \infty)$ if we choose the negative sign, while $u \in [0, R/2]$ for the positive sign. We find the relation

$$\frac{dr^2}{\left(1 \mp \frac{r^2}{R^2}\right)^2} = \frac{du^2}{1 \pm 4\frac{u^2}{R^2}}, \quad (36)$$

such that the line element becomes

$$ds^2 = -dt^2 + a^2(t) \left(\frac{du^2}{1 - \kappa u^2} + u^2 d\varphi^2 \right), \quad (37)$$

which corresponds to the line element of curved FLRW universes with negative/positive spatial curvature $\kappa = \mp 4/R^2$. Therein, the size of the condensate R determines the value of the scalar curvature κ , which allows the latter to be engineered in practice. Moreover, as the scale factor $a^2(t)$ is antiproportional to the coupling $\lambda(t)$ [cf. Eq. (33)], decreasing (increasing) the coupling corresponds to an expanding (contracting) universe.

Interestingly, one can recover a flat FLRW universe without any additional variable transformation when realizing a homogeneous background density profile $n_0 = \text{const.}$, such that the radial dependent prefactor in the spatial line element (32) is absent. This is typically fulfilled in a box trap or in a sufficiently small region around the center of a (harmonic) trap.

Let us mention that for a (possibly inverted) harmonic trap $f(r) = \pm r^2$, the acoustic metric becomes

$$ds^2 = -dt^2 + a^2(t) \left(1 \mp \frac{r^2}{R^2}\right)^{-1} (dr^2 + r^2 d\varphi^2), \quad (38)$$

requiring the coordinate transformation to be of the form

$$u(r) = \frac{r}{\left(1 \mp \frac{r^2}{R^2}\right)^{1/2}}. \quad (39)$$

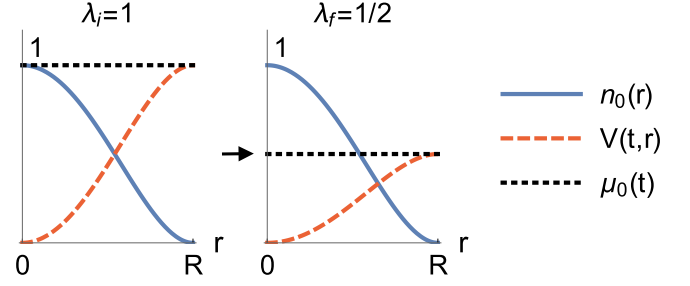


FIG. 1. The density profile $n_0(r) = \bar{n}_0(1 - r^2/R^2)^2$ (blue solid curve) is shown together with the corresponding time-dependent trapping potential $V(t, r)$ (red dashed curve) and chemical potential $\mu_0(t)$ (black dotted line). Note that we have set $\bar{n}_0 = 1$. Decreasing the coupling $\lambda_i = 1 \rightarrow \lambda_f = \lambda_i/2 = 1/2$ and changing the trapping potential $V(t, r)$ accordingly leads to a stationary background density profile $n_0(r)$. In order to illustrate this we set all SI units to 1.

Expanding the denominator of the radial differential up to quadratic order in the new radial coordinate u yields

$$\frac{dr^2}{1 \mp \frac{r^2}{R^2}} = \frac{du^2}{\left(1 \pm \frac{u^2}{R^2}\right)^2} \approx \frac{du^2}{1 \pm 2\frac{u^2}{R^2}}, \quad (40)$$

which is a reasonable approximation in a large region around the center of the trap. Then, one can also arrive at (37) for $\kappa = \mp 2/R^2$, such that the harmonic trap produces curved FLRW universes in a macroscopic region around the center of the trap. Typically, the approximation works well up to $r \approx 0.4R$. However, for the mapping to be exact within the acoustic approximation, the trapping potential has to be of the form (19).

Let us remark here that different forms of optical trap profiles can be realized with a digital micromirror device. This includes inverted trap shapes in some bounded region of space. For more details on a concrete experimental realization, we refer to our companion paper [51].

E. Models of spatially curved spacetimes

The relation between the density profiles (19) and the spatially curved FLRW universes is illustrated in Fig. 2(a). Thereupon, let us further comment on the different sets of spatial coordinates and their geometric meaning.

The spatial FLRW line element (37) is written in terms of reduced-circumference polar coordinates in two spatial dimensions (u, φ) , which is a convenient choice also in cosmology. The radial coordinate transformation in (35) corresponds (up to a factor of 2) to the transformation between reduced-circumference polar coordinates and polar coordinates in the polar plane ($r \leq R, \varphi$) for $\kappa > 0$, or in the Poincaré disk model ($r \leq R, \varphi$) for $\kappa < 0$. Hence, the laboratory line element (34) describes at every instance of time t , depending on spatial curvature, a polar disk or a Poincaré disk.

The arising spatially curved geometries in the laboratory coordinates (r, φ) may be understood from the more intuitive spherical and hyperboloid models, for which we make a distinction of cases. For the positively curved universe ($\kappa > 0$), we start from three-dimensional Euclidean space \mathbb{R}^3 with

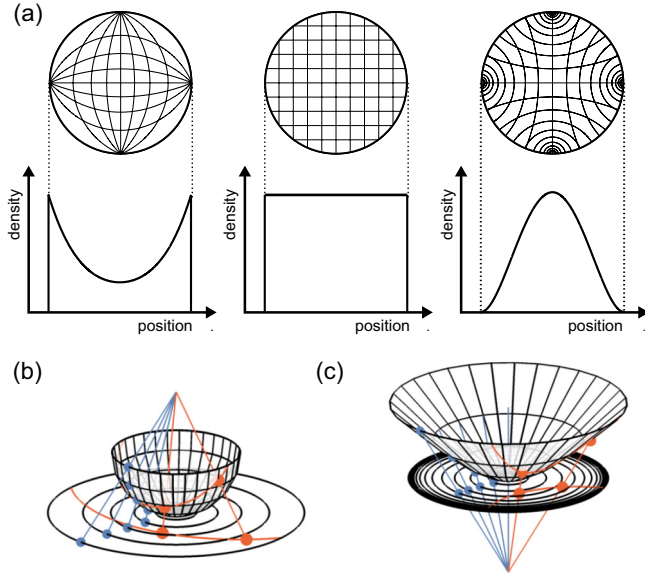


FIG. 2. (a) The one-to-one correspondence between particular radially symmetric density profiles and geometries of FLRW universes is shown, with lattices emphasizing spatial curvature. (b) The blue points on a positively curved universe represented as a half-sphere embedded in three-dimensional Euclidean space are projected onto a polar disk via the blue straight lines. The two red points are connected by a geodesic (red line). (c) Similar setup for a negatively curved universe shown as a hyperboloid embedded in three-dimensional Minkowski space, which is projected onto the Poincaré disk.

cartesian coordinates (X, Y, Z) and line element

$$ds^2 = dX^2 + dY^2 + dZ^2. \quad (41)$$

A two-sphere of radius $R/2$ is embedded in this space via the equation

$$R^2/4 = X^2 + Y^2 + Z^2. \quad (42)$$

Points on the sphere can be represented by two angles $\theta' \in [0, \pi]$, $\varphi' \in [0, 2\pi)$, which can be mapped to the global coordinates via

$$(X, Y, Z) = R/2 (\sin \theta' \cos \varphi', \sin \theta' \sin \varphi', \cos \theta'). \quad (43)$$

The induced metric on the two-sphere reads

$$ds^2 = R^2/4 (d\theta'^2 + \sin^2 \theta' d\varphi'^2), \quad (44)$$

which corresponds to an intuitive representation of a positively curved space [cf. Fig. 2(b)]. However, the two-sphere can also be mapped to the laboratory picture, i.e., the polar disk with coordinates (r, φ) , via a stereographic projection from the north pole $(0, 0, R/2)$ onto the disk located at the south pole $(0, 0, -R/2)$ [illustrated with blue lines connecting points on the sphere and on the plane in Fig. 2(b)]. Then, the laboratory coordinates are related to the coordinates in S^2 by

$$(r, \varphi) = \left(R \cot \frac{\theta'}{2}, \varphi' \right), \quad (45)$$

and we obtain the spatial part of the FLRW line element in the laboratory (34), with positive sign.

In the case of the negatively curved universe ($\kappa < 0$), we have to start from the three-dimensional Minkowski space \mathbb{M}^3 instead [52]. Adapting the cartesian coordinates (X, Y, Z) from before leads to a line element of the form

$$ds^2 = dX^2 + dY^2 - dZ^2, \quad (46)$$

with an additional minus sign compared to (41). Then, the upper hyperboloid can be embedded in this space through [cf. Fig. 2(c)]

$$-R^2/4 = X^2 + Y^2 - Z^2, \quad (47)$$

with $Z > 0$. On the hyperboloid, we choose a pseudoangle $\sigma' \in [0, \infty)$ instead of an angle $\theta' \in [0, \pi]$, but keep the azimuthal angle $\varphi' \in [0, 2\pi)$. We can express the global coordinates in terms of the latter coordinates as

$$(X, Y, Z) = R/2 (\sinh \sigma' \cos \varphi', \sinh \sigma' \sin \varphi', \cosh \sigma'), \quad (48)$$

leading to an induced metric

$$ds^2 = R^2/4 (d\sigma'^2 + \sinh^2 \sigma' d\varphi'^2) \quad (49)$$

on the hyperboloid. Finally, we recover the laboratory coordinates (r, φ) by a projection of the hyperboloid onto the Poincaré disk located at the south pole of the hyperboloid, i.e., at $(0, 0, R/2)$, using the apex $(0, 0, -R/2)$ of the lower hyperboloid [not shown in Fig. 2(c)] as the base point. This projection is sketched with blue straight lines in Fig. 2(c). We obtain the relation

$$(r, \varphi) = \left(R \coth \frac{\sigma'}{2}, \varphi' \right), \quad (50)$$

and the spatial part of the FLRW line element (34) with a minus sign for the metric in the Poincaré disk.

F. Phonon trajectories

To exemplify the influence of spatial curvature on the dynamics of acoustic excitations in the BEC, we consider the motion of a radially outmoving wave packet starting from the center of the trap. Phonons follow null geodesics in an acoustic spacetime, so we look for trajectories with $ds^2 = 0$.

We proceed with the general line element (32), which is expressed in terms of the radial coordinate in the laboratory r . For radial geodesics we have $d\varphi = 0$; this, together with $ds^2 = 0$, leads to the simple differential equation

$$\frac{dt}{a(t)} = \frac{dr}{\sqrt{1 - f(r)/R^2}}, \quad (51)$$

with the initial condition $r(t=0) = 0$. The three different types of spatial curvature are generated by

$$f(r) = \begin{cases} -2r^2 - r^4/R^2 & \text{for } \kappa > 0 \\ 0 & \text{for } \kappa = 0 \\ +2r^2 - r^4/R^2 & \text{for } \kappa < 0, \end{cases} \quad (52)$$

so the equation of motion (51) has general solutions of the form

$$r(t) = R \begin{cases} \tan z(t) & \text{for } \kappa > 0 \\ z(t) & \text{for } \kappa = 0 \\ \tanh z(t) & \text{for } \kappa < 0, \end{cases} \quad (53)$$

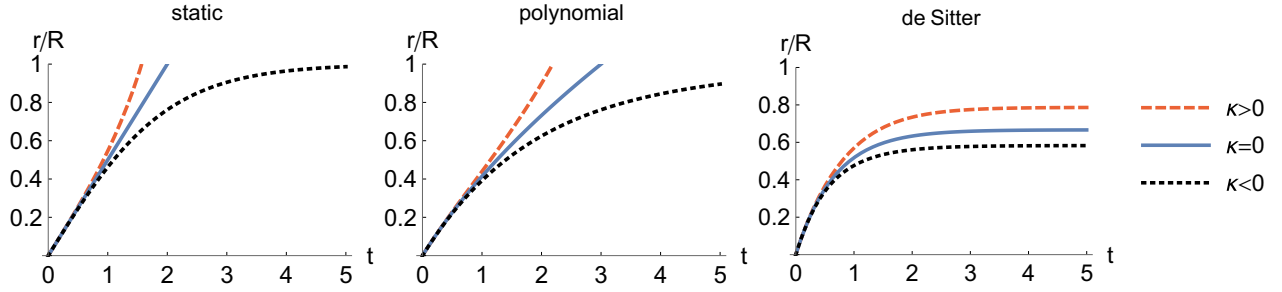


FIG. 3. The trajectories of radially outmoving phonons for the trap profiles given in Eq. (52) are shown for a static situation (left panel, with values $Q = 2, t_0 = -1, R = 1$), a polynomial scale factor $a(t) = Q(t - t_0)^{1/2}$ (middle panel, with values $Q = 2, t_0 = -1, R = 1$) and a de Sitter type scale factor (right panel, with values $a_0 = 1, H = 1.5, R = 1$). Clearly, the spatial curvature influences the bending of the curves, with stronger/weaker bending for open (black dotted line)/closed (red dashed line) universes compared to the flat one (blue solid line). Again, for convenience, we work with dimensionless parameters.

where the argument $z(t)$ can be obtained from the scale factor $a(t)$ via

$$z(t) = \frac{1}{R} \int_0^t \frac{dt'}{a(t')}. \tag{54}$$

For a quadratic trap profile, $f(r) = \pm r^2$, we would obtain \sin (\sinh) instead of \tanh (\tan) in Eq. (53).

It is of particular interest to consider polynomial scale factors. To explicitly allow for expanding as well as contracting scenarios, we write

$$a(t) = Q |t - t_0|^\gamma, \tag{55}$$

where $Q = a(t = 0) |t_0|^{-\gamma} > 0$ and t_0 are free parameters to be tuned in experiments. The latter family of scale factors comprises the analogs of radiation dominated ($\gamma = 2/3$) and matter dominated ($\gamma = 1$) universes. Note that the units of the parameter Q depend on the power γ .

For the polynomial scale factors with $\gamma \neq 1$, we find

$$z(t) = \frac{1}{QR} \frac{\text{sgn}(t - t_0) |t - t_0|^{1-\gamma} + \text{sgn}(t_0) |t_0|^{1-\gamma}}{1 - \gamma}, \tag{56}$$

which is shown in the middle panel of Fig. 3 for $\gamma = 1/2$. For the specific case $\gamma = 0$ corresponding to a static situation (cf. left panel in Fig. 3), we get

$$z(t) = \frac{t}{QR}, \tag{57}$$

while $\gamma = 1$ corresponds to

$$z(t) = \frac{1}{QR} \ln \frac{|t - t_0|}{|t_0|}. \tag{58}$$

Another interesting example is the de Sitter universe, which is characterized by the scale factor

$$a(t) = a_0 e^{Ht}, \tag{59}$$

where H denotes the Hubble parameter and $a_0 = a(t = 0)$ is now the initial scale factor. In this case, we find

$$z(t) = \frac{1}{a_0 HR} (1 - e^{-Ht}). \tag{60}$$

The resulting trajectories are depicted in the right panel of Fig. 3. The quantitative influence of the spatial curvature parameter κ is clearly visible.

III. PARTICLE PRODUCTION

We now turn to the phenomenon of particle production, which arises when the spacetime geometry becomes time dependent. We develop a formalism to access particle production experimentally within the FLRW cosmology paradigm and consider all three types of spatial curvature engineered via (52).

A. Klein-Gordon equation and mode functions

Let us start with the action (28) for the fluctuation field ϕ . Varying the latter using Eq. (37) leads to a Klein-Gordon equation

$$0 = \partial_\mu (\sqrt{g} g^{\mu\nu} \partial_\nu \phi) = 2a(t)\dot{a}(t)\dot{\phi} + a^2(t)\ddot{\phi} - \Delta\phi, \tag{61}$$

where $\dot{f} \equiv \partial_t f$ denotes the partial derivative with respect to time t . The exact form of the Laplace-Beltrami operator depends on the spatial curvature (see below).

For spatially curved universes with $\kappa > 0$, we transform the radial coordinate u to an angle θ . It is convenient to extend from the half sphere to the full sphere such that $\theta \in [0, \pi)$. Similarly, for $\kappa < 0$ we can introduce the pseudoangle $\sigma \in [0, \infty)$ and for $\kappa = 0$ we work with an infinitely extended disk, $u \in [0, \infty)$. In summary, we work with a radial coordinate θ, u or σ defined by

$$u = \begin{cases} \frac{\sin \theta}{\sqrt{|\kappa|}} & \text{for } \kappa > 0 \\ u & \text{for } \kappa = 0 \\ \frac{\sinh \sigma}{\sqrt{|\kappa|}} & \text{for } \kappa < 0. \end{cases} \tag{62}$$

In these coordinates, one has

$$\sqrt{g} = a^2(t) \times \begin{cases} \frac{\sin \theta}{|\kappa|} & \text{for } \kappa > 0 \\ u & \text{for } \kappa = 0 \\ \frac{\sinh \sigma}{|\kappa|} & \text{for } \kappa < 0, \end{cases} \tag{63}$$

and the isotropic Laplace-Beltrami operator in Eq. (61) takes the simple form [53–55]

$$\Delta = \begin{cases} |\kappa| \left[\frac{1}{\sin \theta} \partial_\theta (\sin \theta \partial_\theta) + \frac{1}{\sin^2 \theta} \partial_\varphi^2 \right] & \text{for } \kappa > 0 \\ \partial_u^2 + \frac{1}{u} \partial_u + \frac{1}{u^2} \partial_\varphi^2 & \text{for } \kappa = 0 \\ |\kappa| \left[\frac{1}{\sinh \sigma} \partial_\sigma (\sinh \sigma \partial_\sigma) + \frac{1}{\sinh^2 \sigma} \partial_\varphi^2 \right] & \text{for } \kappa < 0. \end{cases} \tag{64}$$

The Laplace-Beltrami operator can be diagonalized through an eigenvalue equation

$$\Delta \mathcal{H}_{km}(u, \varphi) = h(k) \mathcal{H}_{km}(u, \varphi), \quad (65)$$

where we have introduced the radial wave numbers k and l , which are related by $k = \sqrt{|\kappa|}l$, and the azimuthal wave number m , with the ranges

$$\begin{aligned} l \in \mathbb{N}_0, m \in \{-l, \dots, l\} & \text{ for } \kappa > 0 \\ k \in \mathbb{R}_0^+, m \in \mathbb{Z} & \text{ for } \kappa = 0 \\ l \in \mathbb{R}_0^+, m \in \mathbb{Z} & \text{ for } \kappa < 0, \end{aligned} \quad (66)$$

along with sets of complete and orthonormal eigenfunctions

$$\mathcal{H}_{km}(u, \varphi) = \begin{cases} Y_{lm}(\theta, \varphi) & \text{for } \kappa > 0 \\ X_{km}(u, \varphi) & \text{for } \kappa = 0 \\ W_{lm}(\sigma, \varphi) & \text{for } \kappa < 0. \end{cases} \quad (67)$$

Here, $Y_{lm}(\theta, \varphi)$ are an adapted version of the spherical harmonics,

$$Y_{lm}(\theta, \varphi) = \sqrt{\frac{(l-m)!}{(l+m)!}} e^{im\varphi} P_{lm}(\cos \theta), \quad (68)$$

with $P_{lm}(\cos \theta) = (-1)^m P_l^m(\cos \theta)$ denoting the associated Legendre polynomials. Besides this sign, the choice in (68) differs by a factor $\sqrt{4\pi}/\sqrt{2l+1}$ from the standard definition of the spherical harmonics. For the flat two-dimensional space, one may use polar waves defined in terms of Bessel functions of the first kind:

$$X_{km}(u, \varphi) = e^{im\varphi} J_m(ku). \quad (69)$$

Finally, $W_{lm}(\sigma, \varphi)$ are the eigenfunctions for $\kappa < 0$, which are given by

$$W_{lm}(\sigma, \varphi) = (-i)^m \frac{\Gamma(il+1/2)}{\Gamma(il+m+1/2)} e^{im\varphi} P_{il-1/2}^m(\cosh \sigma), \quad (70)$$

wherein $P_{il-1/2}^m(\cosh \sigma)$ are conical functions corresponding to analytically continued Legendre functions. The functions in Eqs. (68)–(70) are normalized with respect to a scalar product as discussed in detail in Ref. [43].

With these conventions, the eigenvalues $h(k)$ of the Laplace-Beltrami operator Δ defined in Eq. (64) read

$$h(k) = \begin{cases} -k(k + \sqrt{|\kappa|}) & \text{for } \kappa > 0 \\ -k^2 & \text{for } \kappa = 0 \\ -(k^2 + \frac{1}{4}|\kappa|) & \text{for } \kappa < 0, \end{cases} \quad (71)$$

with the relation $k = \sqrt{|\kappa|}l$ understood in the two spatially curved cases. Note that $h(k=0)$ is only nonvanishing for the open universe, $\kappa < 0$, and $\sqrt{|\kappa|}/2$ acts there like an effective mass gap.

The fluctuation field ϕ is quantized as usual such that it obeys the (equal time) bosonic commutation relations,

$$\begin{aligned} & [\phi(t, u, \varphi), \pi(t, u', \varphi')] \\ &= i\hbar \delta(\varphi - \varphi') \times \begin{cases} \delta(\theta - \theta') & \text{for } \kappa > 0 \\ \delta(u - u') & \text{for } \kappa = 0 \\ \delta(\sigma - \sigma') & \text{for } \kappa < 0, \end{cases} \end{aligned} \quad (72)$$

where

$$\pi(t, u, \varphi) = \frac{\delta \Gamma_2[\phi]}{\delta \dot{\phi}} = \hbar^2 \sqrt{g} \dot{\phi} \quad (73)$$

denotes the conjugate momentum field.

To solve the linearized equation of motion (61) for the different classes of universes, we expand the quantum field ϕ in terms of the corresponding eigenfunctions of the Laplace-Beltrami operator (67),

$$\phi(t, u, \varphi) = \int_{k,m} [\hat{a}_{km} \mathcal{H}_{km}(u, \varphi) v_k(t) + \hat{a}_{km}^\dagger \mathcal{H}_{km}^*(u, \varphi) v_k^*(t)], \quad (74)$$

and similar for the conjugate momentum field $\pi(t, u, \varphi)$.

Therein, we used the abbreviation

$$\int_{k,m} = \begin{cases} \sum_{l=0}^{\infty} |\kappa| \frac{l+1/2}{2\pi} \sum_{m=-l}^l & \text{for } \kappa > 0 \\ \int \frac{dk}{2\pi} k \sum_{m=-\infty}^{\infty} & \text{for } \kappa = 0 \\ \int \frac{dl}{2\pi} |\kappa| l \tanh(\pi l) \sum_{m=-\infty}^{\infty} & \text{for } \kappa < 0 \end{cases} \quad (75)$$

for the two-dimensional momentum integral. Also, we have introduced creation and annihilation operators \hat{a}_{km}^\dagger and \hat{a}_{km} , respectively, which fulfill the bosonic commutation relations

$$\begin{aligned} & [\hat{a}_{km}^\dagger, \hat{a}_{k'm'}^\dagger] = [\hat{a}_{km}, \hat{a}_{k'm'}] = 0, \\ & [\hat{a}_{km}, \hat{a}_{k'm'}^\dagger] = 2\pi \delta_{mm'} \begin{cases} \frac{\delta_{ll'}}{|\kappa|(l+1/2)} & \text{for } \kappa > 0 \\ \frac{\delta(k-k')}{k} & \text{for } \kappa = 0 \\ \frac{\delta(l-l')}{|\kappa|l \tanh(\pi l)} & \text{for } \kappa < 0, \end{cases} \end{aligned} \quad (76)$$

together with the time-dependent mode functions $v_k(t)$ and $v_k^*(t)$.

Combining the latter statements, we find from the Klein-Gordon equation (61) the so-called mode equation

$$\ddot{v}_k(t) + 2 \frac{\dot{a}(t)}{a(t)} \dot{v}_k(t) - \frac{h(k)}{a^2(t)} v_k(t) = 0. \quad (77)$$

For given initial conditions at some point in time, one can determine $v_k(t)$ by solving Eq. (77). Note that the influence of the spatial curvature κ is fully encoded in $h(k)$. On the scales relevant for typical experiments, i.e., for $R \sim 10^{-5}$ m, $h(k)$ turns out to be practically independent of the spatial curvature κ for $k/\sqrt{\tilde{n}_0} \gtrsim 0.1$.

The mode functions are further constrained as a result of the canonical commutation relation (72), the orthonormality properties of the functions $\mathcal{H}_{km}(u, \varphi)$ (see Ref. [43]), and the bosonic commutation relations fulfilled by the creation and annihilation operators (76), leading to a normalization condition in terms of the Wronskian,

$$\text{Wr}[v_k, v_k^*] = a^2(t) \hbar [v_k \dot{v}_k^* - \dot{v}_k v_k^*] = i. \quad (78)$$

By using (77), one can show that (78) is fulfilled at all times when it is fulfilled at one point in time.

Let us note here that (77) is a second-order differential equation and (78) is just a single constraint, so the mode functions $v_k(t)$ are not fixed completely. In fact, different choices of mode functions correspond to different choices of creation and annihilation operators, and they are related by Bogoliubov transformations. Note that the quantum field ϕ

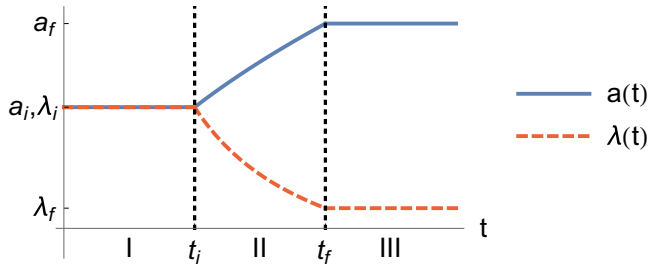


FIG. 4. The time dependence of the scale factor $a(t)$ (blue solid line) and the coupling $\lambda(t)$ (red dashed line) are shown for the three regions I–III. Up to t_i , both are held constant, while they become time dependent in region II (the plot above correspond to a polynomial expansion with $\gamma = 1/2$, $Q = m/\bar{n}_0 = 1$, and $t_0 = 0$, setting all units to 1), this time dependence leads to particle production, observed in the stationary region III for $t > t_f$.

in (74) is independent of this choice. This is important to understand particle production, and will be discussed next.

B. Bogoliubov transformations

Let us start by considering a situation (in the following called region I) where the scale factor is constant, $a(t) = a_i$. In that case, one has a preferred choice of mode functions $v_k(t)$ given by oscillatory modes,

$$v_k^I(t) = \frac{\exp(-i\omega_k^I t)}{a_i \sqrt{2\hbar\omega_k^I}}, \quad (79)$$

with positive frequency $\omega_k^I = \sqrt{-\hbar(k)}/a_i$. Associated with this choice of mode functions are operators \hat{a}_{km} and \hat{a}_{km}^\dagger that annihilate and create the corresponding phonons, and a vacuum state $|\Omega\rangle$ that has no such excitations:

$$\hat{a}_{km} |\Omega\rangle = 0. \quad (80)$$

The state $|\Omega\rangle$ describes the ground state of a (weakly interacting) BEC with no excitations. More generally, one may also take some other state as a starting point, for example with fixed temperature T .

Let us now assume that at some time t_i the scale factor $a(t)$ becomes time dependent, until it becomes constant again at time t_f . For the intermediate times $t_i < t < t_f$ (called region II in the following), the mode functions are determined as solutions of Eq. (77), with initial conditions at $t = t_i$ set by continuity to the solution (79). We stress that for a time-dependent scale factor (in region II), the solution $v_k(t)$ obtained in this way will not be of the oscillatory form (79). As a consequence, the notions of vacuum states and (quasi)particles become more involved. Mathematically, this is related to the absence of a global timelike Killing vector field in that region, which would allow to define positive frequency waves.

We concentrate on an experimental procedure sketched in Fig. 4. Keeping in mind that the scale factor $a(t)$ is controlled by the inverse coupling $\lambda(t)$ according to (33), one may first engineer certain initial values a_i and λ_i in a time interval I up to t_i . Then, the coupling $\lambda(t)$ is varied over time in time interval II, which simulates a FLRW universe with time-

dependent scale factor $a(t)$. Finally, the variation is stopped at $t_f = t_i + \Delta t$, corresponding to a stationary FLRW universe with scale factor a_f in time interval III.

Let us then consider times $t > t_f$ where we assume that the scale factor is again constant, $a(t) = a_f$ (region III). Here one can again find solutions of Eq. (77) in terms of modes with positive frequencies,

$$u_k^{\text{III}}(t) = \frac{\exp(-i\omega_k^{\text{III}} t)}{a_f \sqrt{2\hbar\omega_k^{\text{III}}}}, \quad (81)$$

where now $\omega_k^{\text{III}} = \sqrt{-\hbar(k)}/a_f$. Associated to these modes are operators \hat{b}_{km} and \hat{b}_{km}^\dagger and a corresponding vacuum state $|\Psi\rangle$, such that

$$\hat{b}_{km} |\Psi\rangle = 0. \quad (82)$$

It is now important to note that the mode functions $v_k(t)$ obtained from extending the solution in region I to region II and then into region III will actually be a linear superposition of positive and negative frequency solutions, so one can write

$$u_k = \alpha_k v_k + \beta_k v_k^*, \quad v_k = \alpha_k^* u_k - \beta_k u_k^*, \quad (83)$$

with the complex-valued and time-independent Bogoliubov coefficients α_k and β_k . From the normalization condition (78) applied to $u_k(t)$ follows that the coefficients need to satisfy $|\alpha_k|^2 - |\beta_k|^2 = 1$. In terms of the Wronskian defined in (78), one has

$$\alpha_k = \text{Wr}[u_k, v_k^*]/i, \quad \beta_k = -\text{Wr}[u_k, v_k]/i. \quad (84)$$

For completeness, we also mention the relation between the two sets of creation and annihilation operators:

$$\hat{b}_{km} = \alpha_k^* \hat{a}_{km} - \beta_k^* (-1)^m \hat{a}_{k,-m}^\dagger. \quad (85)$$

In particular it follows that the state $|\Omega\rangle$, which is initially a vacuum state in the sense of Eq. (80), is not an empty state with respect to the excitations annihilated by the operators \hat{b}_{km} . This is the essence of particle production due to a time dependent scale factor $a(t)$.

The task is then to solve the mode equation [Eq. (77)] in all three regions I–III and to identify the Bogoliubov coefficients α_k and β_k through Eqs. (84), from which all following quantities can be derived.

C. Rescaled density contrast: Correlation function and spectrum

To access the phenomenon of particle production experimentally, we introduce a rescaled density contrast

$$\delta_c(t, u, \varphi) = \sqrt{\frac{n_0(u)}{\bar{n}_0^3}} [n(t, u, \varphi) - n_0(u)], \quad (86)$$

where $n(t, u, \varphi) = |\Phi(t, u, \varphi)|^2$ denotes the full condensate density and \bar{n}_0 is the density in the center of the trap. In this way, the rescaled density contrast is dimensionless, and using Eqs. (5) as well as (31) one has to leading order $\delta_c \sim \partial_t \phi$. Note here that for a box potential the given prefactor is constant, while for other trapping potentials, such as those put forward in Eqs. (19), it has a substantial dependence on u in the outer regions of the trap.

In the following, we consider the equal time two-point correlation function of the rescaled density contrast after the expansion has ceased, $t \geq t_f$, i.e.,

$$\mathcal{G}_{nn}(t; u, u', \varphi, \varphi') = \langle \delta_c(t, u, \varphi) \delta_c(t, u', \varphi') \rangle, \quad (87)$$

which is a typical observable in modern ultracold atom experiments. One can show that in leading order in fluctuating fields, where we can assume $\langle n(t, u, \varphi) \rangle = n_0(u)$, the latter is proportional to the connected two-point correlation function

$$L = \begin{cases} \frac{1}{\sqrt{|\kappa|}} \cos^{-1}(\cos \theta \cos \theta' + \sin \theta \sin \theta' \cos(\varphi - \varphi')) & \text{for } \kappa > 0 \\ [u^2 + u'^2 - 2uu' \cos(\varphi - \varphi')]^{1/2} & \text{for } \kappa = 0 \\ \frac{1}{\sqrt{|\kappa|}} \cosh^{-1}(\cosh \sigma \cosh \sigma' - \sinh \sigma \sinh \sigma' \cos(\varphi - \varphi')) & \text{for } \kappa < 0, \end{cases} \quad (90)$$

and through (88) the observable defined in (86) acquires the symmetries of the FLRW universe,

$$\mathcal{G}_{nn}(t; u, \varphi, u', \varphi') \equiv \mathcal{G}_{nn}(t, L). \quad (91)$$

We proceed with the evaluation of this correlation function through (89) within the FLRW universe paradigm using the Bogoliubov transformations introduced in Sec. III B. This leads to

$$\mathcal{G}_{nn}(t, L) = \frac{\hbar a_f}{\bar{n}_0 m} \int_k \mathcal{F}(k, L) \sqrt{-h(k)} S_k(t), \quad (92)$$

where we introduced the spectrum of fluctuations

$$S_k(t) = \frac{1}{2} + N_k + \Delta N_k(t), \quad (93)$$

as the momentum space representation of the rescaled density contrast two-point correlation function.

Therein, we have the expected occupation number of phonon excitations per mode

$$N_k = \langle \Omega | \hat{b}_{km}^\dagger \hat{b}_{km} | \Omega \rangle = |\beta_k|^2, \quad (94)$$

and the time-dependent contribution

$$\Delta N_k(t) = \text{Re}[c_k e^{2i\omega_k t}], \quad (95)$$

wherein

$$c_k = -(-1)^m \langle \Omega | \hat{b}_{km}^\dagger \hat{b}_{k,-m}^\dagger | \Omega \rangle = \alpha_k \beta_k. \quad (96)$$

Furthermore, we used the abbreviation

$$\int_k = \begin{cases} \sum_{l=0}^{\infty} |\kappa| \frac{l+1/2}{2\pi} & \text{for } \kappa > 0 \\ \int \frac{dk}{2\pi} k & \text{for } \kappa = 0 \\ \int \frac{dl}{2\pi} |\kappa| l \tanh(\pi l) & \text{for } \kappa < 0, \end{cases} \quad (97)$$

and the integration kernels

$$\mathcal{F}(k, L) = \begin{cases} P_l(\cos(L\sqrt{|\kappa|})) & \text{for } \kappa > 0 \\ J_0(kL) & \text{for } \kappa = 0 \\ P_{l-1/2}(\cosh(L\sqrt{|\kappa|})) & \text{for } \kappa < 0, \end{cases} \quad (98)$$

for the different spatial curvatures specified by κ .

of time derivatives of fields

$$\mathcal{G}_{nn}(t; u, u', \varphi, \varphi') = \frac{\hbar^2 m}{\lambda_1^2 \bar{n}_0^3} \mathcal{G}_{\dot{\phi}\dot{\phi}}(t, L), \quad (88)$$

where

$$\mathcal{G}_{\dot{\phi}\dot{\phi}}(t, L) = \frac{1}{2} \langle \{\dot{\phi}(t, u, \varphi), \dot{\phi}(t, u', \varphi')\} \rangle_c. \quad (89)$$

The relation given in (88) is a result of the normalization chosen in (86).

Moreover, as a consequence of the spatial homogeneity of FLRW universes, two-point correlation functions do not depend separately on the two spatial positions (u, φ) and (u', φ') , but only on the comoving distance L between them,

We can rewrite the spectrum of fluctuations (93) using (95) and Euler's formula

$$S_k(t) = \frac{1}{2} + N_k + |c_k| \cos(2\omega_k t + \theta_k), \quad (99)$$

where

$$\theta_k = \text{Arg}(c_k) \quad (100)$$

denotes the phase corresponding to the momentum mode k .

It is useful to note at this point that N_k and ΔN_k defined in (94) and (95) with the relations (84) are invariant under phase transformations on the mode functions $v_k(t) \rightarrow e^{i\lambda_k} v_k(t)$, $u_k(t) \rightarrow e^{i\mu_k} u_k(t)$, if one also takes into account $e^{2i\omega t} \rightarrow e^{-2i\mu_k} e^{2i\omega t}$ in Eq. (95). These phases should not be observable.

Also, following Refs. [56,57], one can show that entanglement between modes with opposite wave numbers can be witnessed in the two-mode squeezed state of relevance whenever $\Delta N_k > N_k$. The latter was recently observed experimentally in Ref. [58] within a homogeneous two-dimensional BEC after quenching the time-dependent coupling $\lambda(t)$ to negative values and back. We leave a similar analysis within the FLRW universe paradigm for future work.

Moreover, it is important to note that a two-point correlation function of fields as defined in (89) shows an ultraviolet divergence [3]. Consequently, the rescaled density contrast correlation function (92) has to be regularized. In the context of a BEC, a regularization arises naturally as the readout of the density contrast is limited by the precision of the measurement apparatus. Moreover, the acoustic approximation that we use here is a low momentum effective description that loses validity in the ultraviolet regime.

To solve this problem, which is well-known in cosmology, one may work with smeared-out fields

$$\Phi(t, \mathbf{r}) = \int d^2 r' W(\mathbf{r} - \mathbf{r}') \phi(t, \mathbf{r}'), \quad (101)$$

with a window function $W(\mathbf{r} - \mathbf{r}')$. The latter can be normalized according to

$$\int d^2 r' W(\mathbf{r}') = 1. \quad (102)$$

In momentum space, this window function plays the role of an ultraviolet regulator. We end up with a regularized expression for the rescaled density contrast correlation function

$$G_{mn}(t, L) = \frac{\hbar a_f}{\hbar_{0m}} \int_k \mathcal{F}(k, L) \sqrt{-h(k)} S_k(t) \tilde{f}_G(k), \quad (103)$$

where $\tilde{f}_G(k) = \tilde{W}^*(k) \tilde{W}(k)$ corresponds to the absolute square of the Fourier transformed window function.

In the following, we work with a window function of Gaussian form in position space (as a function of the comoving distance), such that in the absence of spatial curvature:

$$\tilde{f}_G(k) = \tilde{W}^*(k) \tilde{W}(k) = e^{-w^2 k^2}. \quad (104)$$

D. Stimulated particle production

An initial state at time t_i with nonvanishing occupation number, such as a thermal state, would lead to stimulated particle production [59]. This leads to a generalization of the expressions derived above.

Assuming that the expected occupation number of quasiparticles originally present in the mode k is given by

$$N_k^{\text{in}} = \langle \hat{a}_{km}^\dagger \hat{a}_{km} \rangle, \quad (105)$$

the total expected number of quasiparticles after expansion would be given by

$$N_k = N_k^{\text{in}} + |\beta_k|^2 (1 + 2N_k^{\text{in}}), \quad (106)$$

where the last term corresponds to the stimulated production. Similarly, $\Delta N_k(t)$ is generalized to

$$c_k = \alpha_k \beta_k (1 + 2N_k^{\text{in}}). \quad (107)$$

As an example, we will consider a thermal state, characterized by an initial occupation number of the form

$$N_k^{\text{in}}(T) = \frac{1}{e^{\hbar \omega_k / (k_B T)} - 1}, \quad (108)$$

where T denotes the temperature.

In the following, to set a temperature scale, we use the critical temperature T_c of an ideal gas in an anisotropic trap. In particular, we consider a ratio between longitudinal and radial trapping frequencies that elicit the emergence of a 2D condensate [60]. This critical temperature is given by

$$T_c = \frac{\hbar \omega}{k_B} \left(\frac{N}{\zeta(2)} \right)^{1/2}, \quad (109)$$

where N is the total number of atoms.

IV. EFFECTS OF EXPANSION

Let us now focus on particle production as the main trait of an expanding spacetime, we do this within the developed formalism for a set of cosmological situations. In particular,

we consider the spectrum of fluctuations together with the rescaled density contrast correlation function and discuss the outcome of various experimental scenarios. If not stated differently, the experimental values are taken from Appendix B.

A. Polynomial scale factors with various expansion rates and holding times

We base our analysis on polynomial scale factors of powers γ according to Eq. (55), which comprise accelerating ($\gamma = 3/2$), uniform ($\gamma = 1$), and decelerating ($\gamma = 1/2$) expansions, and look into different expansion rates Δt and hold times after the expansion has ceased.

We study in Fig. 5 the effect of increasing the expansion duration (at fixed ratio $a_f/a_i = \sqrt{6}$) and obtain an analogous prediction to a cosmological situation: for slower expansion the characteristic features of the power spectrum appear at smaller wave numbers. This can be read out from the change in the shape of the spectrum in the first row of Fig. 5. It can also be seen that a decelerating expansion leads to slightly higher contrast in the spectrum compared to accelerating or uniform expansion. Furthermore, at large momenta, the spectrum converges to the ground state or vacuum expression. In the second row of Fig. 5, we show the manifestation of these features in position space, through the correlation function $G_{mn}(t, L)$ given in (103). On top of a strong (diverging at $L = 0$) anticorrelation coming from features of the ground state or vacuum, we see an anticorrelation-correlation pair at finite distances. The magnitude of this pair of correlations decreases with slower expansion rates, and is highest for a decelerating scenario.

The evolution after expansion is given in the two lower rows of Fig. 5. After a simulated expansion, done by a 2 ms ramp, has ceased, the spectrum shifts to lower momenta, and oscillates in time for each k mode around N_k , with a period corresponding to the frequency of each mode. A node in the spectrum appears for a particular value of k which is not excited in the process of particle production ($\beta_k = 0$). This precise feature is present only for the case of uniform expansion, and will be discussed further in Sec. IV D.

Complementary, the position space evolution exhibits a decreasing magnitude of correlation-anticorrelation pair through time, along with a propagation to larger distances. In the short range, we also see a correlation build up as a reaction to the expansion dynamics. The group of correlations propagates at twice the speed of sound [Eq. (27) at the center of the trap], as phonons travel away from each other. The chosen width for convolution (here $w = 0.5 \mu\text{m}$) influences the shape of $G_{mn}(t, L)$ but not the position of the peaks, with the only exception being the vacuum anticorrelation, which goes to $L = 0$ in the limit of vanishing width. Robust features with respect to changes of the width are discussed in Sec. IV E.

B. Initial thermal state

Together with an initial thermal state comes about the phenomenon of stimulated particle production described in Sec. III D. Given the divergence of the statistical distribution (108) at low momenta, there is a large occupation of soft modes also after the expansion, in contrast with the outcome

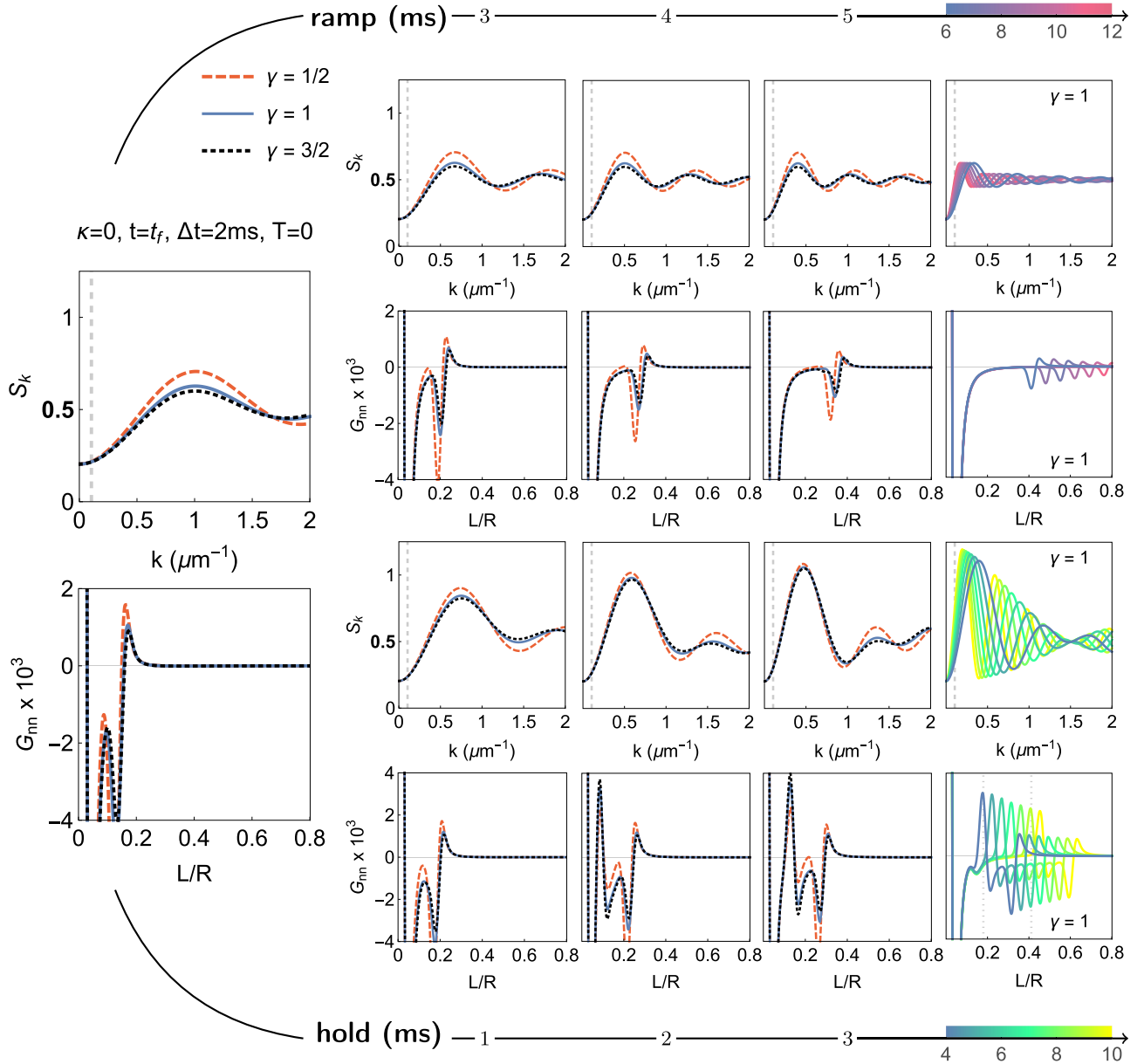


FIG. 5. Spectrum of fluctuations S_k as a function of the radial wave number k together with its corresponding rescaled density contrast correlation function $G_m(L)$ [cf. Eq. (103)] as a function of the comoving distance L measured in units of the parameter R . Both are shown for various types of polynomial expansions (decelerating $\gamma = 1/2$, uniform $\gamma = 1$, and accelerating $\gamma = 3/2$). Left column: Spectrum and correlation function right at the end of expansion. The dependence on different expansion rates Δt is depicted above, and evolution after expansion is shown below. At the level of the spectra, one can appreciate that a slower expansion moves power to smaller wave numbers, whereas for faster expansions, more modes with higher momenta get excited. The hold-time dependence shows how this power is evolving with time, in favor of the lower momentum modes. At the level of the correlation functions, one can see that both faster expansion rates Δt and decelerated expansions ($\gamma < 1$) lead to stronger short-range anticorrelations. The propagation of the spatial correlations in time after the expansion has ceased is governed by the speed of sound in the condensate. In the lower row, we show this: The correlation first builds up to a maximum, in this case reached at 3 ms holding time, and then it travels through the condensate at twice the speed of sound. In the lower right panel, we highlight through dotted lines the distance traversed after 5 ms by moving at twice the speed of sound. In all the momentum space plots, a gray vertical dashed line indicates the low k limit at inverse condensate size. The position space results are obtained after regularization with a Gaussian window function of width $w = 0.5 \mu\text{m}$.

for vanishing initial temperature. Since stimulated particle production is present for any state above the ground state with $T = 0$, the study of this phenomenon is crucial when comparing to realistic experimental situations. On the other hand, the question arises whether the initial state in a concrete experiment is actually thermal. In any case, the phenomenon

of particle production can help to investigate the properties of the initial state in an experimental setting.

In Fig. 6, we investigate stimulated particle production for three different initial temperatures in fractions of T_c , at the level of both, the spectrum, and the rescaled density contrast correlation function as a function of hold time.

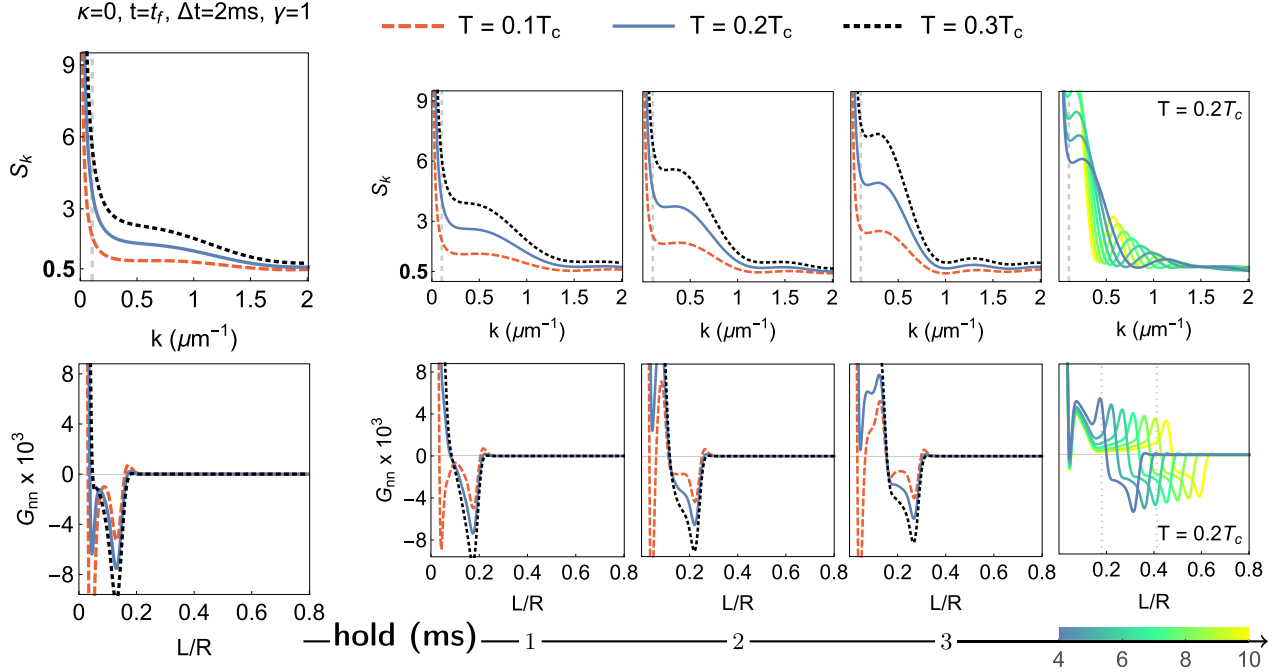


FIG. 6. Effect of initial temperature, leading to stimulated particle production: It can be seen that in this case, the number of excited soft momenta is large, in contrast to particle production from the vacuum; note also that the spectrum S_k diverges for $k \rightarrow 0$ as a consequence of the bosonic nature of gapless phonons at vanishing spatial curvature. After the expansion has ceased, the power apparently moves toward lower momentum modes and the spectrum distribution oscillates around $S_k = (1/2 + |\beta_k|^2)(1 + 2N_k^{\text{in}})$. Regarding position space, a finite initial occupation enhances anticorrelations and suppresses correlations. The short-range correlation that builds up after the expansion has ceased is also enhanced and the correlations propagate again at twice the speed of sound, indicated through dotted lines in the bottom right panel. The two-point rescaled density contrast converges at long times to a thermal state, plus a finite contribution from the excited modes, determined by $|\beta_k|^2$. In all the momentum space plots, a gray vertical dashed line indicates the low k limit at inverse condensate size. The position space results given here correspond to a Gaussian convolution of $w = 0.5 \mu\text{m}$ standard deviation.

C. Spatial curvature

We showed in Sec. IID that different types of trapping potentials induce acoustic spacetimes with different emergent spatial curvatures. In the formalism employed in Sec. III A, the effects of spatial curvature are carried into the shape of Laplace-Beltrami’s operator, its eigenfunctions, and its eigenvalues. Regarding time evolution in momentum space [cf. Eq. (77)], spatial curvature enters in fact only through the eigenvalue spectrum. Here, the features of spatial curvature are equivalent to posing different boundary conditions on the eigenvalue equation, and do not go further than that. A further dependence on spatial curvature arises in the integral transform from momentum to position space [cf. Eq. (98)].

As expected, the effect of curvature on the spectrum of fluctuations is often negligible, but can be tuned to a higher impact when decreasing the condensate radius. Something similar happens to the rescaled density contrast, where differences are unimportant, even at small radii; this is shown in Fig. 7. In the presence of an initial thermal state, this situation could change, given that the Bose-Einstein distribution (108) differs for different dispersion relations. In particular, for negative curvature, N_k^{in} is bounded at $k = 0$, as a consequence of an acquired gap in the dispersion relation. This was investigated and no particular differences were found at different curvatures.

D. Time evolution of momentum modes and robust features in momentum space

As we see overall in Fig. 5, the qualitative differences related to different exponents γ in the scale factor could be difficult to appreciate experimentally when looking into the complete spectrum and rescaled density contrast. Nevertheless, one can look into details of the spectrum, and through them, validate the particle production nature of the experimental outcomes, and its dependence on different expansion histories.

We consider first the time evolution of the spectra for certain modes in regions II and III (cf. Fig. 8), that is, during and after the dynamic change of the scale factor; there we observe that, independently of the polynomial power of the scale factor, the phononic modes corresponding to small wave numbers are suppressed by the expansion, which is consistent with Fig. 5. Moreover, the time evolution of each momentum mode shows a slight dependence on the expansion history, which is most evident for a particular mode, at $k = 1.51 \mu\text{m}^{-1}$, that remains in its vacuum value after uniform expansion ($\gamma = 1$), given that this characteristic is not present for any mode in nonuniform expansions.

This precise feature is also explicit in the phase θ_k that each mode acquires after expansion, defined in (100), which we consider next in Fig. 9. There, we see that the phases of

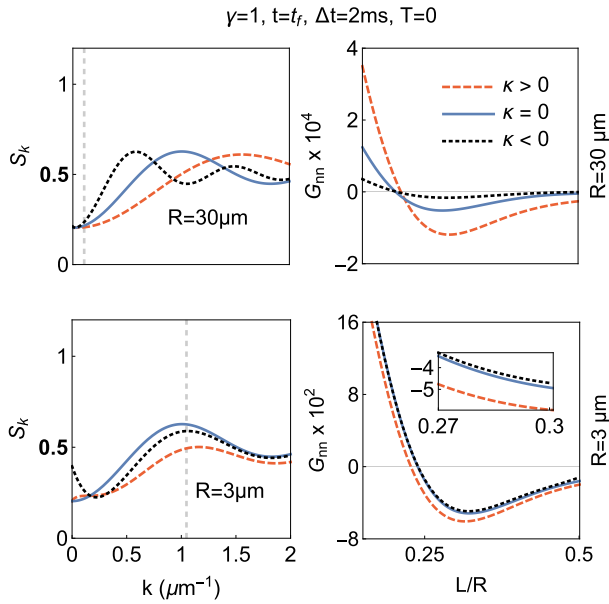


FIG. 7. Effect of different trapping potentials (inverted harmonic, box, harmonic), which convey different spatial curvatures (positive, flat, negative; respectively). In the upper row, we show the outcome for a fixed atom number, so the density at the center of the trap depends on the shape of the trap [cf. (17) and (52)]; this renders visible differences for both the spectrum S_k and the rescaled density contrast G_{mn} (obtained with a Gaussian convolution of width $w = 4 \mu\text{m}$). However, if the density at the center is taken to be the same for all trap shapes, the spatial curvature κ influences the shape of the spectrum S_k only at low momentum modes and provided that R is sufficiently small, as depicted in the lower row. The differences between rescaled density contrast correlations for the closed, flat, and open universe are barely visible even when $R = 3 \mu\text{m}$. Additionally, for the chosen convolution width ($w = 0.4 \mu\text{m}$), the vacuum sector dominates in position space. An inset into the correlation function shows that the results for each curvature fall one above the other: this is a width-independent feature.

each wave number k strongly depend on whether there is a decelerated, uniform, or accelerated expansion. In the case of uniform expansion, there are phase jumps appearing at each mode where β_k turns out to be zero. To emphasize, due to the shape of expansion, β_k is never zero for $\gamma \neq 1$. It is worthwhile to note that phases as a function of k also give an insight into the expansion duration Δt .

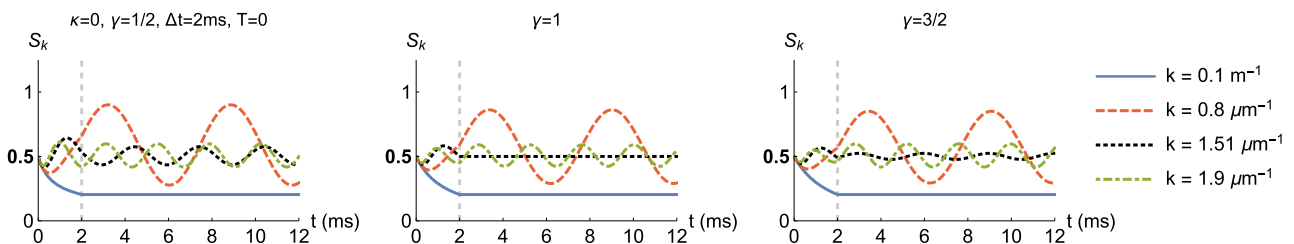


FIG. 8. Time evolution of the spectrum S_k for four radial wave numbers k from $t = 0$ (setting $t_i = 0$) up to $t = t_f + 10$ ms. Emphasized through a vertical dashed line is the moment the expansion ceases, i.e., $t = t_f$. The low-momentum modes are suppressed by the expansion and they almost become static when the expansion has ceased. For higher momentum modes, the amplitude at the time of expansion is greater in the case of a decelerating scenario. Depending on the duration of expansion, there are always certain modes (in this case $k = 1.51 \mu\text{m}^{-1}$) which remain in their vacuum state after expansion for the $\gamma = 1$ situation. These same modes exhibit the greatest difference in amplitude between the $\gamma = 1/2$ and $\gamma = 3/2$ situations.

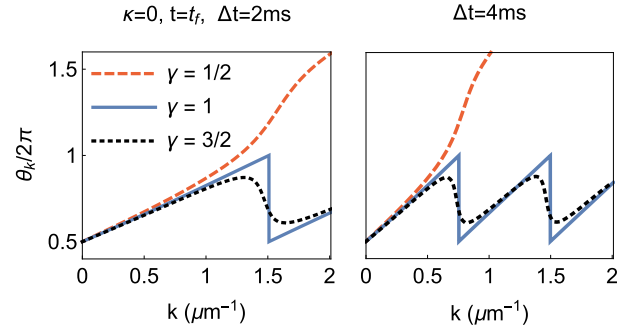


FIG. 9. Phases θ_k [cf. (100)] of each k mode after expansion for three different scale factors. We see an important qualitative difference in behavior depending on the choice of γ : for $\gamma = 1$ and $\gamma = 3/2$ the phase remains in a range of $(0, \pi)$, in particular, in the $\gamma = 1$ case the phase is a linear function of k . Also, for this case there is a π jump which appears if and only if $N_k = 0$, that is, when a particular mode is not excited as a result of expansion. The other two scale factors do not exhibit this feature. In contrast, for $\gamma = 1/2$ the phase increases continuously in the complete range $(0, 2\pi)$. In all cases, a slower expansion rate allows for a greater phase growth.

E. Window function dependence and robust features in position space

Given that any computation of the rescaled density contrast correlation function requires an ultraviolet regulator in the form of a window or test function, we wish to find features of the latter which are robust against variations in the standard deviation w of the Gaussian family of window functions we have chosen in Eq. (104). This is not only an interesting task by itself but also paves the ground for a quantitative comparison to experiments.

To that end, we study the positions of the second minimum—the first minimum is just the vacuum contribution—and the first maximum of the correlation function. More precisely, we investigate the aforementioned positions as a function of expansion duration Δt for different widths w , for the particular case of $\gamma = 1/2$. The results are shown in Fig. 10: We find that the influence of the width w is negligible with regards to the slope of the curves, rendering position versus expansion duration a robust observable. Also in Fig. 10, the rescaled density contrast correlation function $G_{mn}(t, L)$ is shown for different widths w . The resolution w

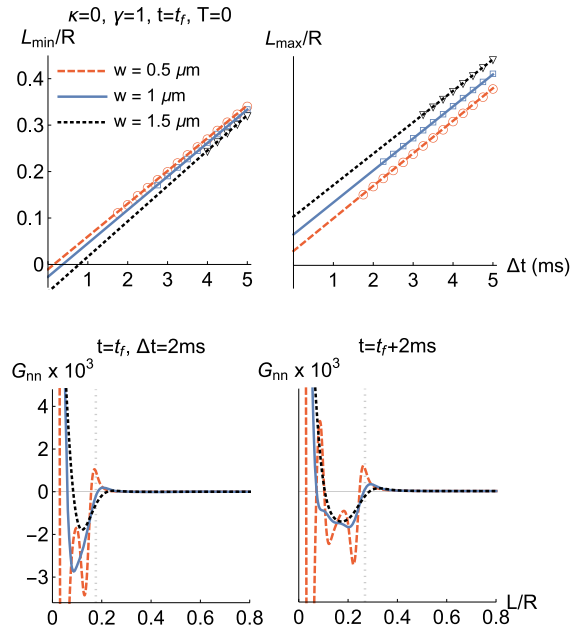


FIG. 10. Upper row: Positions of the second minimum L_{\min}/R (left) and first maximum L_{\max}/R (right) of the rescaled density contrast correlation function $G_{nn}(t, L)$ as a function of the expansion duration Δt for various widths w . The linear fits exhibit slopes robust against w and almost fall on top of each other in the former case. Lower row: $G_{nn}(t, L)$ for various widths w at the time the expansion has ceased (left panel) and two milliseconds after (right panel). Most sensitive to the choice of w are the position and magnitude of the vacuum anticorrelation. The position of the group of correlations coming from particle production is relatively robust against w , but the peaks tend to disappear as the width grows closer to the healing length $\xi \approx 1.6 \mu\text{m}$. However, the group of correlations moves with twice the speed of sound, independent of the width w (indicated by a gray dotted line).

determines the short-length $L < 0.1R$ behavior of the two-point correlator indicating the need for robust features.

Moreover, let us report that we have also investigated the amplitudes of the maximum and the minimum and their ratio but did not find a similar form of robustness.

V. CONCLUSION AND OUTLOOK

In summary, we have derived a correspondence between phonons in a $2 + 1$ dimensional BEC in various radially symmetric trapping potentials and massless scalar particles in spatially curved FLRW universes. As opposed to common literature, this correspondence was established starting from a nonrelativistic action and describing phononic excitations in terms of the real and imaginary parts of the fluctuations on top of the mean field.

Furthermore, we investigated the phenomenon of particle production in momentum and in position space for various experimentally accessible scenarios. We showed that a suitably rescaled density contrast correlation function is to leading order proportional to a correlator within the FLRW universe paradigm. As a consequence of rescaling, spatial homogeneity and isotropy carried over to the density contrast correlation function. Looking into experimental feasibility, we

have shown that the phases of momentum modes and the positions of maxima and minima in the correlation function serve as robust observables and are distinguishable for different dynamics in the scale factor.

In future theoretical work, it would be interesting to extend our approach from $d = 2 + 1$ to $d = 3 + 1$ dimensions, which should be straightforward. Also, one may want to study more general excitation fields, involving spin degrees of freedom, or modes with gapped excitation spectrum. Also a generalization to the full Bogoliubov spectrum beyond the acoustic approximation can be of interest for some questions.

Another interesting direction could be to investigate other expansions specified by the scale parameter, allowing for a simulation of various epochs of expanding or contracting universes. In particular, one may study the de Sitter universe in the context of inflation or even a cyclic universe, probably exhibiting additional features such as parametric resonance.

Moreover, one may investigate particle production from a quantum information theoretic perspective. More precisely, entanglement between modes of opposite momenta may be analyzed for spatially curved universes, extending the work of Refs. [56,57].

Most importantly, it is of great interest to apply our methods to concrete ultracold atom experiments. In particular, as the rescaled density contrast correlation function serves as a typical observable, our work paves the ground to an extensive experimental investigation of particle production. We report on the experimental realization of our proposal in Ref. [51].

ACKNOWLEDGMENTS

The authors would like to thank Simon Brunner and Finn Schmutte for useful discussions. This work is supported by the Deutsche Forschungsgemeinschaft (DFG, German Research Foundation) under Germany's Excellence Strategy EXC 2181/1390900948 (the Heidelberg STRUCTURES Excellence Cluster), under Project-ID 273811115 - SFB 1225 ISOQUANT and under Project-ID FL 736/3-1, furthermore by the ERC Advanced Grant Horizon 2020 Entangle-Gen (Project-ID No. 694561). N.S.K. is supported by the Deutscher Akademischer Austauschdienst (DAAD, German Academic Exchange Service) under the Länderbezogenes Kooperationsprogramm mit Mexiko: CONACYT Promotion (No. 57437340). A.P.L. is supported by the MIU (Ministerio de Universidades, Spain) Fellowship No. FPU20/05603 and the MICINN (Ministerio de Ciencia e Innovación, Spain) Project No. PID2019-107394GB-I00 (AEI/FEDER, UE). N.L. acknowledges support by the Studienstiftung des Deutschen Volkes.

APPENDIX A: FULL BOGOLIUBOV DISPERSION RELATION

To assess the validity of the acoustic approximation, it is also interesting to perform calculations in full Bogoliubov theory for excitations in weakly interacting Bose-Einstein gases. This is applicable, in particular, for homogeneous BECs and for static situations such as quantum fluctuations around the ground state, or in thermal equilibrium. An extension of this formalism to time-dependent situations and more

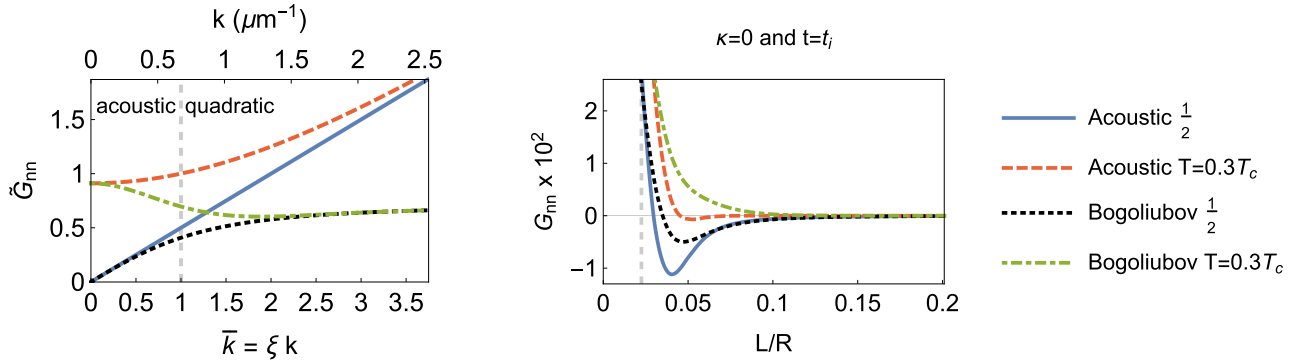


FIG. 11. The influence of the full Bogoliubov dispersion relation (A1) and an initial temperature $T = 0.3T_c$ is discussed at initial time $t = t_i$ for the rescaled density contrast correlation function in momentum space (left panel) and in position space (right panel). For small momenta $k \ll 1/\xi$ (indicated by the dashed vertical line), the Bogoliubov dispersion approaches the acoustic result (dashed versus dot-dashed and solid versus dotted curves), while for large momenta $k \gg 1/\xi$ the temperature dependence vanishes due to the exponential fall-off of the Bose-Einstein distribution $N_k^{\text{in}}(T)$ for large k (dashed versus solid and dotted versus dot-dashed curves). Moreover, the correlation function is clearly influenced by a nonvanishing temperature $T = 0.3T_c$, while a dependence on whether one includes the full Bogoliubov dispersion is subleading due to the Gaussian cutoff in momentum space as $w \approx \xi$ at initial time.

general trapping potentials is possible, but beyond our scope in the present paper.

The Bogoliubov dispersion relation for quasiparticles reads

$$\omega_k = \frac{\hbar}{2m} \sqrt{k^2(k^2 + 2/\xi^2)}. \quad (\text{A1})$$

This features a transition at the healing length

$$\xi = \frac{\hbar}{\sqrt{2m\lambda n_0}}, \quad (\text{A2})$$

such that for small wave numbers $k \ll 1/\xi$ the dispersion relation is linear, $\omega_k = ck$, with the speed of sound c as defined in (27), while for large wave numbers $k \gg 1/\xi$ it becomes quadratic, $\omega_k \rightarrow \hbar k^2/(2m) + \lambda n_0/\hbar$.

For an initial thermal state with temperature $T < T_c$ introduced in (108), the spectrum of fluctuations is given by

$$S_k(t_i) = \frac{1}{2} + N_k^{\text{in}}(T), \quad (\text{A3})$$

while the rescaled density contrast correlation function evaluates to [61]

$$G_m(t_i, L) = \frac{2}{\bar{n}_0} \int_k k J_0(kL) \sqrt{\frac{k^2}{k^2 + 2/\xi^2}} S_k(t_i) \tilde{f}_G(k), \quad (\text{A4})$$

where the linear dispersion relation $\sqrt{-\hbar(k)} = k$ has been replaced by the corresponding expression of the full Bogoliubov dispersion relation (A1). Note that in the acoustic limit $k \ll 1/\xi$, we obtain Eq. (103) with a_f replaced by a_i . The integrand and its respective correlator are shown in Fig. 11 for the acoustic vacuum and the Bogoliubov vacuum with and without an initial temperature $T = 0.3T_c$.

APPENDIX B: EXPERIMENTAL SETUP

The plots shown in Sec. IV are computed for the following experimental parameters, setting $t_i = 0$, out of convenience. The condensate consists of $N = 15 \times 10^3$ potassium atoms of mass $m = 6.47008 \times 10^{-26}$ kg and extends up to a radius $R = 30 \times 10^{-6}$ m. The longitudinal trapping frequency is $1.75 \times 10^3 \text{ s}^{-1}$ while the initial and final s -wave scattering lengths are $a_s(t_i) = 300a_0$ and $a_s(t_f) = 50a_0$, respectively, where a_0 denotes the Bohr radius. The 2D critical temperature for an anisotropic trap is calculated for these values at initial time, and yields $T_c = 82.41 \times 10^{-9}$ K. Moreover, the regularization for the correlation functions is carried out with a Gaussian of inverse standard deviation $w = 5 \times 10^{-7}$ m.

-
- [1] L. Parker, Quantized fields and particle creation in expanding universes. I, *Phys. Rev.* **183**, 1057 (1969).
- [2] N. D. Birrell and P. C. W. Davies, *Quantum Fields in Curved Space*, Cambridge Monographs on Mathematical Physics (Cambridge University Press, Cambridge, 1982).
- [3] V. Mukhanov and S. Winitzki, *Introduction to Quantum Effects in Gravity* (Cambridge University Press, Cambridge, 2007).
- [4] S. Weinberg, *Cosmology* (Oxford University Press, Oxford, 2008).
- [5] C. Barceló, S. Liberati, and M. Visser, Analogue gravity, *Living Rev. Relativ.* **14**, 3 (2011).
- [6] M. Visser, C. Barceló, and S. Liberati, Analogue models of and for gravity, *Gen. Relativ. Gravit.* **34**, 1719 (2002).
- [7] M. Novello, M. Visser, and G. E. Volovik, eds., *Artificial Black Holes* (World Scientific Publishing, Singapore, 2002).
- [8] G. E. Volovik, *The Universe in a Helium Droplet* (Oxford University Press, Oxford, 2009).
- [9] W. G. Unruh, Experimental Black-Hole Evaporation? *Phys. Rev. Lett.* **46**, 1351 (1981).
- [10] W. G. Unruh, Sonic analogue of black holes and the effects of high frequencies on black hole evaporation, *Phys. Rev. D* **51**, 2827 (1995).
- [11] C. Barceló, S. Liberati, and M. Visser, Probing semiclassical analog gravity in Bose-Einstein condensates with widely tunable interactions, *Phys. Rev. A* **68**, 053613 (2003).

- [12] P. O. Fedichev and U. R. Fischer, Gibbons-Hawking Effect in the Sonic de Sitter Space-Time of an Expanding Bose-Einstein Condensed Gas, *Phys. Rev. Lett.* **91**, 240407 (2003).
- [13] P. O. Fedichev and U. R. Fischer, “Cosmological” quasiparticle production in harmonically trapped superfluid gases, *Phys. Rev. A* **69**, 033602 (2004).
- [14] U. R. Fischer, Quasiparticle universes in Bose-Einstein condensates, *Mod. Phys. Lett. A* **19**, 1789 (2004).
- [15] U. R. Fischer and R. Schützhold, Quantum simulation of cosmic inflation in two-component Bose-Einstein condensates, *Phys. Rev. A* **70**, 063615 (2004).
- [16] M. Uhlmann, Y. Xu, and R. Schützhold, Aspects of cosmic inflation in expanding Bose-Einstein condensates, *New J. Phys.* **7**, 248 (2005).
- [17] E. A. Calzetta and B. L. Hu, Early Universe quantum processes in BEC collapse experiments, *Int. J. Theor. Phys.* **44**, 1691 (2005).
- [18] P. Jain, S. Weinfurter, M. Visser, and C. W. Gardiner, Analog model of a Friedmann-Robertson-Walker universe in Bose-Einstein condensates: Application of the classical field method, *Phys. Rev. A* **76**, 033616 (2007).
- [19] S. Weinfurter, P. Jain, M. Visser, and C. W. Gardiner, Cosmological particle production in emergent rainbow spacetimes, *Class. Quantum Grav.* **26**, 065012 (2009).
- [20] A. Prain, S. Fagnocchi, and S. Liberati, Analogue cosmological particle creation: Quantum correlations in expanding Bose-Einstein condensates, *Phys. Rev. D* **82**, 105018 (2010).
- [21] N. Bilić and D. Tolić, FRW universe in the laboratory, *Phys. Rev. D* **88**, 105002 (2013).
- [22] S. Weinfurter, S. Liberati, and M. Visser, Analogue model for quantum gravity phenomenology, *J. Phys. A: Math. Gen.* **39**, 6807 (2006).
- [23] S. Liberati, M. Visser, and S. Weinfurter, Analogue quantum gravity phenomenology from a two-component Bose-Einstein condensate, *Class. Quantum Grav.* **23**, 3129 (2006).
- [24] S. Liberati, M. Visser, and S. Weinfurter, Naturalness in an Emergent Analogue Spacetime, *Phys. Rev. Lett.* **96**, 151301 (2006).
- [25] Note that the case of $d = 1 + 1$ spacetime dimensions is somewhat special from a cosmological point of view because the infinite dimensional group of conformal transformations allows mapping all spaces with FLRW metric to flat Minkowski space. Moreover, the spacetime integral of the curvature scalar is a topological invariant (Gauss-Bonnet theorem).
- [26] S. Eckel, A. Kumar, T. Jacobson, I. B. Spielman, and G. K. Campbell, A Rapidly Expanding Bose-Einstein Condensate: An Expanding Universe in the Lab, *Phys. Rev. X* **8**, 021021 (2018).
- [27] M. Wittemer, F. Hakelberg, P. Kiefer, J.-P. Schröder, C. Fey, R. Schützhold, U. Warring, and T. Schaetz, Phonon Pair Creation by Inflating Quantum Fluctuations in an Ion Trap, *Phys. Rev. Lett.* **123**, 180502 (2019).
- [28] M. Visser, Acoustic black holes: horizons, ergospheres and Hawking radiation, *Class. Quantum Grav.* **15**, 1767 (1998).
- [29] C. Barceló, S. Liberati, and M. Visser, Towards the observation of Hawking radiation in Bose-Einstein condensates, *Int. J. Mod. Phys. A* **18**, 3735 (2003).
- [30] L. J. Garay, J. R. Anglin, J. I. Cirac, and P. Zoller, Sonic Analog of Gravitational Black Holes in Bose-Einstein Condensates, *Phys. Rev. Lett.* **85**, 4643 (2000).
- [31] L. J. Garay, J. R. Anglin, J. I. Cirac, and P. Zoller, Sonic black holes in dilute Bose-Einstein condensates, *Phys. Rev. A* **63**, 023611 (2001).
- [32] J. Rodríguez-Laguna, L. Tarruell, M. Lewenstein, and A. Celi, Synthetic Unruh effect in cold atoms, *Phys. Rev. A* **95**, 013627 (2017).
- [33] J. Hu, L. Feng, Z. Zhang, and C. Chin, Quantum simulation of Unruh radiation, *Nat. Phys.* **15**, 785 (2019).
- [34] C. Gooding, S. Biermann, S. Erne, J. Louko, W. G. Unruh, J. Schmiedmayer, and S. Weinfurter, Interferometric Unruh Detectors for Bose-Einstein Condensates, *Phys. Rev. Lett.* **125**, 213603 (2020).
- [35] B. Horstmann, B. Reznik, S. Fagnocchi, and J. I. Cirac, Hawking Radiation from an Acoustic Black Hole on an Ion Ring, *Phys. Rev. Lett.* **104**, 250403 (2010).
- [36] S. Weinfurter, E. W. Tedford, M. C. J. Penrice, W. G. Unruh, and G. A. Lawrence, Measurement of Stimulated Hawking Emission in an Analogue System, *Phys. Rev. Lett.* **106**, 021302 (2011).
- [37] J. Steinhauer, Observation of quantum Hawking radiation and its entanglement in an analogue black hole, *Nat. Phys.* **12**, 959 (2016).
- [38] J. R. Muñoz de Nova, K. Golubkov, V. I. Kolobov, and J. Steinhauer, Observation of thermal Hawking radiation and its temperature in an analogue black hole, *Nature (London)* **569**, 688 (2019).
- [39] J.-C. Jaskula, G. B. Partridge, M. Bonneau, R. Lopes, J. Ruaudel, D. Boiron, and C. I. Westbrook, Acoustic Analog To The Dynamical Casimir Effect in a Bose-Einstein Condensate, *Phys. Rev. Lett.* **109**, 220401 (2012).
- [40] M. J. Jacquet, S. Weinfurter, and F. König, The next generation of analogue gravity experiments, *Phil. Trans. R. Soc. A* **378**, 20190239 (2020).
- [41] S. Floerchinger and C. Wetterich, Functional renormalization for Bose-Einstein condensation, *Phys. Rev. A* **77**, 053603 (2008).
- [42] L. H. Heyen and S. Floerchinger, Real scalar field, the nonrelativistic limit, and the cosmological expansion, *Phys. Rev. D* **102**, 036024 (2020).
- [43] N. Sánchez-Kuntz, Á. Parra-López, M. Tolosa-Simeón, T. Haas, and S. Floerchinger, Scalar quantum fields in cosmologies with $2 + 1$ spacetime dimensions, *Phys. Rev. D* **105**, 105020 (2022).
- [44] L. Pitaevskii and S. Stringari, *Bose-Einstein Condensation and Superfluidity* (Oxford University Press, Oxford, 2016).
- [45] N. Bogoliubov, On the theory of superfluidity, *J. Phys.* **XI**, 23 (1946).
- [46] E. M. Lifshitz and L. Pitaevskii, *Statistical Physics Part 2* (Pergamon Press, Oxford, 1980).
- [47] E. Madelung, Quantentheorie in hydrodynamischer Form, *Z. Phys.* **40**, 322 (1927).
- [48] Note that usually the divergence of the subsequent equation is referred to as the Euler equation.
- [49] Y. Castin and R. Dum, Bose-Einstein Condensates in Time Dependent Traps, *Phys. Rev. Lett.* **77**, 5315 (1996).
- [50] The acoustic approximation is justified for wave numbers that are small compared to the inverse healing length, $k \ll 1/\xi$, see Appendix A for a more detailed discussion.

- [51] C. Viermann, M. Sparn, N. Liebster, M. Hans, E. Kath, H. Strobel, Á. Parra-López, M. Tolosa-Simeón, N. Sánchez-Kuntz, T. Haas, S. Floerchinger, and M. K. Oberthaler, Quantum field simulator for dynamics in curved spacetime, [arXiv:2202.10399](https://arxiv.org/abs/2202.10399).
- [52] N. Balazs and A. Voros, Chaos on the pseudosphere, *Phys. Rep.* **143**, 109 (1986).
- [53] B. Ratra and P. J. E. Peebles, Inflation in an open universe, *Phys. Rev. D* **52**, 1837 (1995).
- [54] B. Ratra, Inflation in a closed universe, *Phys. Rev. D* **96**, 103534 (2017).
- [55] E. N. Argyres, C. G. Papadopoulos, E. Papantonopoulos, and K. Tamvakis, Quantum dynamical aspects of two-dimensional spaces of constant negative curvature, *J. Phys. A: Math. Gen.* **22**, 3577 (1989).
- [56] S. Robertson, F. Michel, and R. Parentani, Controlling and observing nonseparability of phonons created in time-dependent 1D atomic Bose condensates, *Phys. Rev. D* **95**, 065020 (2017).
- [57] S. Robertson, F. Michel, and R. Parentani, Assessing degrees of entanglement of phonon states in atomic Bose gases through the measurement of commuting observables, *Phys. Rev. D* **96**, 045012 (2017).
- [58] C.-A. Chen, S. Khlebnikov, and C.-L. Hung, Observation of Quasiparticle Pair Production and Quantum Entanglement in Atomic Quantum Gases Quenched to an Attractive Interaction, *Phys. Rev. Lett.* **127**, 060404 (2021).
- [59] E. A. Calzetta and B.-L. B. Hu, *Nonequilibrium Quantum Field Theory*, Cambridge Monographs on Mathematical Physics (Cambridge University Press, Cambridge, 2008).
- [60] F. Dalfovo, S. Giorgini, L. P. Pitaevskii, and S. Stringari, Theory of Bose-Einstein condensation in trapped gases, *Rev. Mod. Phys.* **71**, 463 (1999).
- [61] N. Sánchez-Kuntz and S. Floerchinger, Spatial entanglement in interacting Bose-Einstein condensates, *Phys. Rev. A* **103**, 043327 (2021).